Universidade do Minho
Escola de Engenharia

Marios Filippoupolitis

The South Oculus at Canterbury Cathedral

Julho de 2011

Universidade do Minho
Escola de Engenharia

Marios Filippoupolitis

The South Oculus at Canterbury Cathedral

Advanced Masters in Structural Analysis of Monuments and Historical Constructions

Trabalho efectuado sob a orientação do
Professor Doutor Paulo José Brandão Barbosa Lourenço

Julho de 2011

DECLARATION

Name: Marios Filippoupolitis

Email: marios.filippoupolitis@gmail.com

Title of the MSc Dissertation: The South Oculus at Canterbury Cathedral

Supervisor(s): Paulo B. Lourenco (University of Minho)

Claudio Corallo (The Morton Partnership Ltd)

Year: 2010 - 2011

I hereby declare that all information in this document has been obtained and presented in accordance with academic rules and ethical conduct. I also declare that, as required by these rules and conduct, I have fully cited and referenced all material and results that are not original to this work.

I hereby declare that the MSc Consortium responsible for the Advanced Masters in Structural Analysis of Monuments and Historical Constructions is allowed to store and make available electronically the present MSc Dissertation.

University: University of Minho

Date: 29/07/2011

Signature: _____

To all the people who have supported me during my Civil Engineering studies

ACKNOWLEDGEMENTS

I am grateful to the Dean and Chapter of Canterbury Cathedral for having financed this Thesis and in particular to Leeonie Seliger for the information provided.

Sincere thanks to Ed Morton and Claudio Corallo from The Morton Partnership Ltd for the technical support and assistance along the way.

I would like to give a special acknowledgement to my thesis supervisor, Prof. Paulo B. Lourenco for his guidance and advice during this dissertation. Despite his very hard schedule, he was always available to discuss my queries related to the Thesis.

I would also like to thank the PhD student, Nuno Mendes for his help with the ambiental vibration test and for the general support that he has offered to this dissertation.

Acknowledgements to the S.A.H.C Consortium for the scholarship I received which was an important financial aid for my studies.

Last but not least, I would like to thank Iris Koltsida and Carlos Flores for their support during the Thesis.

ABSTRACT

The South Oculus at Canterbury Cathedral is a wrought iron space frame, consisting of two layers (Ferramenta and Grille) connected by tie bars (Pins). It is in very good condition despite its almost 850 years of history.

The in situ survey of the Cathedral confirmed that the Ferramenta and the external grille are in general in relative good condition with the exception of some local failures. On the contrary, the pins are the most deteriorated part of the structure. An ambiental vibration test was carried out and the modal response of the structure was identified. In order to assess the safety of the oculus with respect to wind load, a model of the structure was built with the finite element software DIANA and calibrated using the results of the experimental campaign.

The non linear analysis of the existing structure resulted in a safety factor of about ten, when compared with the wind load as specified by the EC1. In addition, parametric studies have highlighted the importance of the external grille for the structure and have provided an estimate of the consequences of a further deterioration in terms of the load bearing capacity of the Oculus.

RESUMO

O vitral circular localizado na parede Sul da Catedral de Canterbury corresponde a uma estrutura em ferro forjado composto por duas componentes (grelha externa e estrutura de suporte dos vidros) ligadas por barras ortogonais. Apesar dos 850 anos de história, a estrutura mantém-se em bom estado de conservação.

A inspeção in situ da Catedral confirmou que a estrutura de suporte dos vidros encontra-se, em geral, em bom estado de conservação. Por sua vez, as barras horizontais de ligação das duas componentes apresentam-se como a parte mais deteriorada da estrutura. Além disso, foram realizados ensaios de vibração ambiental, através dos quais foram identificadas as propriedades dinâmicas da estrutura. Tendo por objetivo avaliar a estabilidade do vitral sob a ação do vento, preparou-se um modelo numérico no programa de elementos finitos DIANA. O modelo foi calibrado com recurso aos resultados experimentais obtidos nos ensaios de vibração ambiental.

A análise não linear da estrutura no seu estado atual permitiu concluir que o valor do fator de segurança é cerca de dez, em relação ao valor regulamentar proposto pelo EC1. Além disso, a análise paramétrica realçou a importância da grelha externa no comportamento da estrutura e permitiu ainda estimar as consequências da continuação da deterioração na capacidade de carga do vitral.

ΠΕΡΙΛΗΨΗ

Το ¨μάτι¨ (Oculus, λατ.) του νότιου κλείτους του καθεδρικού ναό στο Canterbury, είναι ένα χωρικό πλαίσιο από σφυρήλατο σίδηρο. Αποτελείται από δύο επίπεδα, ένα εσωτερικό (Ferramenta) το οποίο συγκρατεί το βιτρό και μια εξωτερική εσχάρα (Grille). Η σύνδεση μεταξυ τους γίνεται με τη χρήση μικρών κυλινδρικών συνδετήριων στοιχείων (Pins). Παρά τα περίπου 850 χρόνια της ιστορίας της, η κατασκευή παραμένει σε πολύ καλή κατάσταση.

Η επί τόπου έρευνα έπιβεβαίωσε ότι η Ferramenta και η εξωτερική εσχάρα διατηρούνται γενικά χωρίς κάποια εμφανή σημάδια διάβρωσης, με εξαίρεση κάποιες τοπικες αστοχίες. Αντιθέτως, τα Pins βρέθηκαν ως τα πιο διαβρωμένα τμήματα της κατασκευής. Η ιδιομορφική απόκριση της κατασκευής προσδιορίστηκε με την εκτέλεση ενός ambiental vibration test, τα αποτελέσματα του οποίου χρησιμοποιήθηκαν για την αναβάθμιση του μοντέλου πεπερασμένων στοιχείων, που χρησιμοποιήθηκε για την αποτίμηση της φέρουσας ικανότητας της κατασκευής έναντι ανεμοπιέσεως.

Τα αποτελέσματα της μη – γραμμικής ανάλυσης έδειξαν ότι η κατασκευή στη σημερινή της κατάσταση, συγκρινόμενη με το φορτίο σχεδιασμού που ο EC1 προτείνει για την ανεμοπίεση, δίνει ένα συντελεστή ασφάλειας της τάξης του δέκα. Επιπρόσθετα, οι παραμετρικές αναλύσεις που έγιναν απέδειξαν το σημαντικό ρόλο που έχει η εσχάρα στο μηχανισμό ανάληψης φορτίων, καθώς και τις συνέπειες που θα έχει στη φέρουσα ικανότητα της κατασκευής η περαιτέρω διάβρωση των μελών της.

Table of Contents

List of Figures

List of Tables

1. INTRODUCTION

The oculi are large Romanesque circular windows that are divided into segments by iron armatures and not by stone tracery as happens with the rose windows which replaced the oculi after the mid 13th century (Geddes 2011).

Canterbury Cathedral has two Oculi, one in each of the two east transepts. The South Oculus is a wrought iron space frame structure, built between 1178 and 1180. It consists of two layers, one internal (Ferramenta) and one external (Grille), which are connected by small iron ties, the Pins.

The early date of construction, the large scale (4.47m in diameter) and the design of the original Ferramenta are parameters that make the oculus being considered as a unique structure. Its construction was so effective that the structure has survived over 800 years exposed to the elements, the near collapse of the south gable, pollution, bombing, etc.

Nowadays, the Oculus is in very good condition, considering its age, and although it has experienced some decay that has caused some localized damages, it seems to be performing its function of resisting wind actions very well. The aim of this dissertation is to assess the safety of the South Oculus with respect to wind load and investigate the influence that some parameters have (deterioration, contribution of the grille) in its load bearing capacity.

The thesis is organized as follows:

- Chapter 1: Is this brief introduction to the work.
- Chapter 2: Presents a brief review on Canterbury Cathedral's structural history and on past restoration projects. The Oculus of the South-East Transept is then described in detail.
- Chapter 3: Presents the results of the survey and the non – destructive tests which were carried out in situ at the Cathedral.
- Chapter 4: Describes the model updating procedure according to the results of the experimental campaign.
- Chapter 5: Presents the results of the safety assessment of the structure with respect to wind load and the influence of different parameters in the load bearing behavior of the Oculus.
- Chapter 6: Contains the conclusions of the thesis.

2. CANTERBURY CATHEDRAL AND THE OCULUS IN THE SOUTH TRANSEPT

2.1 Brief review of Canterbury Cathedral from 6th century to Second World War

2.1.1 The Anglo – Saxon period of the Cathedral (597 – 1070)

St Augustine, the first Archbishop of Canterbury, arrived on the coast of Kent as a missionary to England in 597 AD and established the first Cathedral in Canterbury. He came from Rome, sent by Pope Gregory the Great. Between 597 and 1070, the structural history of the Cathedral consists of the following 4 phases: (Collinson, Ramsay and Sparks 2002)

1. The early church of the seventh and eighth century, whether or not it embodied a Roman – British core, seems likely to have been of typical Kentish form. It had an apsidal chancel and a simple nave, which had gradually come to be surrounded on the west, north and south sides by porches (porticus).
2. A separate building, perhaps a baptistery - church, lay within 0.50 m of the south – eastern corner of the nave of the early Cathedral and had also been extended in subsequent periods.
3. A massive enlargement of the Cathedral in the ninth or the tenth century involved widening the foundations (possibly to increase the walls height), incorporating the porticus into side – aisles and doubling the length of both church and aisles by extending them westwards.
4. The final westward extension, and the rebuilding of the west end of the Cathedral, involved the construction of a large western apse with the oratory of St Mary clerestory level and with access by means of hexagonal stair – towers built at the western end of the church.

Nothing of the structure of the Anglo – Saxon Cathedral survives above ground to this day. The church and most of the monastic buildings were destroyed by a great fire on 6 December 1067, and the old buildings were demolished and replaced by Archbishop Lanfranc's new Norman Cathedral. Figure 2-1 shows a plan of the Anglo – Saxon Cathedral and its structural phases.

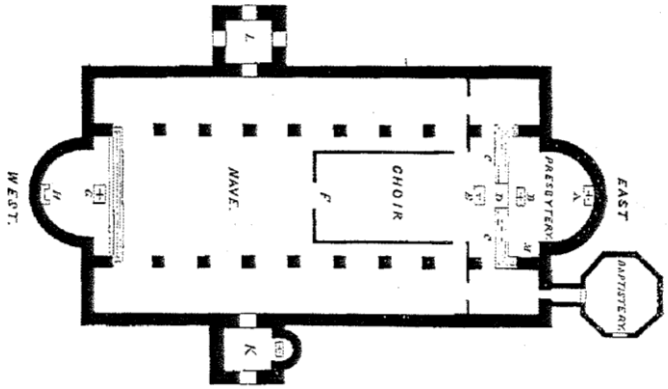

Figure 2-1 The Anglo – Saxon phases of Canterbury Cathedral

2.1.2 The Church of Archbishop Lanfranc

From 1067 until 1077, Archbishop Lanfranc rebuilt the Cathedral as a Norman church. Figure 2-2 shows Canterbury Cathedral as it was at the time of Archbishop Lanfranc. The classic book of *Reverend Willis* entitled *The Architectural History of the Canterbury Cathedral* offers a clear description of the Cathedral in 1077 (Willis 1845). The tower is placed at the center of the church, raised upon the four great pillars. On the west of the tower is the *nave* of the church supported on both sides upon eight pillars and ended by two lofty towers at the west end of the church. On the left and right of the central tower, the two transepts of the Cathedral can be found. In the middle of each transept exists a pillar in order to sustain a vault. Between each transept and the choir, stairs that drive to the cathedral's crypt and to the upper parts of the church, divide this space in two parts.

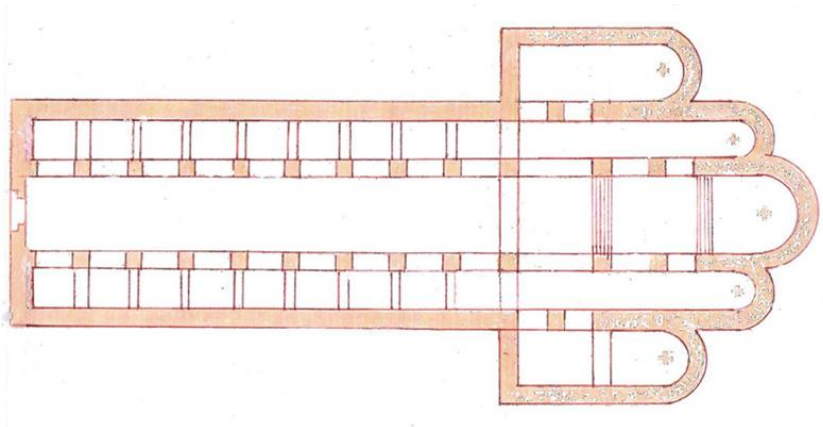

Figure 2-2 Ground floor plan of Canterbury Cathedral in as built by Archbishop Lanfranc in 1077

2.1.3 The new Choir of Archbishop Anselm

After the death of Lanfranc (1089), Canterbury was without an Archbishop for five years and Anselm was consecrated on 4 December 1093. In 1096, Archbishop Anselm started the reconstruction of Lanfranc's choir. The new building entirely replaced Lanfranc's choir and crypt. Whereas Lanfranc's choir had extended some 21 m east of the crossing, the new choir ran 58 m east, with commensurate extension to the north and to the south. Because of the huge dimensions of the new choir, it was required not only to extent the crypt eastward but to reconstruct it totally. This is the vaulted crypt that exists today. The reconstruction work finished on 1130. Figure 2-3 presents Canterbury Cathedral plan after Archbishop's Anselm choir reconstruction.

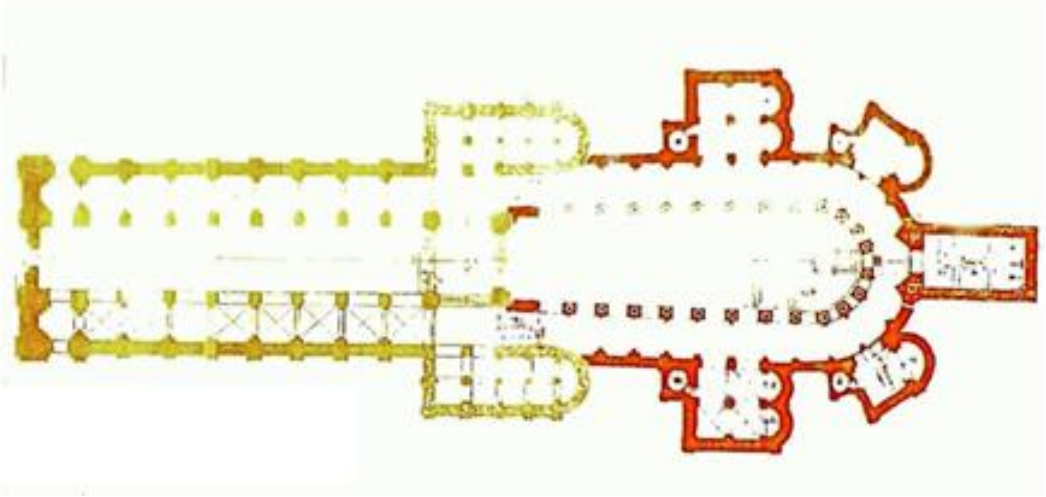

Figure 2-3 Ground floor plan of Canterbury Cathedral after Archbishop's Anselm reconstruction from 1096 until 1130 - The red color indicates the new choir

2.1.4 The New Cathedral (1175 -1184)

The choir of Archbishop Anselm was destroyed by a fire in 1174 and in the following years William of Sens begun building of a third choir. Triforium and clerestory levels were constructed in order to relief the older masonry from the loads of the vaulted stone roof. The new choir had the proportions of the previous one. William the Englishman planned and built the Trinity Chapel and the Corona chapel beyond the limitations of Romanesque into the new architecture of the thirteen century. Figure 2-4 depicts Canterbury Cathedral at the end of 1184 and compares it with the previous two editions of the Cathedral.

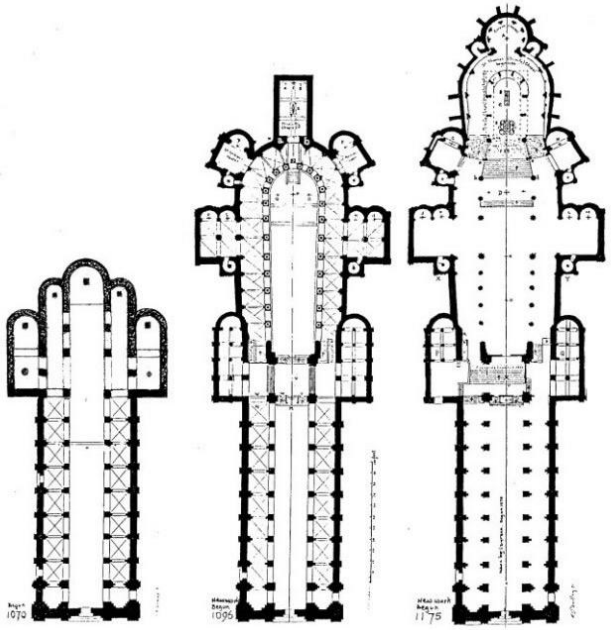

(a) (b) (c)

Figure 2-4 Canterbury Cathedral ground floor development from 1070 to 1184: (a) the Cathedral of Lanfranc - (b) the Cathedral of Anselm - (c) the Cathedral of William of Sens

2.1.5 14th – 19h Centuries

On 1378, Archbishop Sudbury pulled down Lanfranc's nave, intending to rebuild it, but was prevented by his death in 1381. The nave was reconstructed by the Prior Thomas Chillenden (1390 -1411) who gave to the nave the perpendicular style of English Gothic that exists today (Collinson, Ramsay and Sparks 2002) (Figure 2-5).

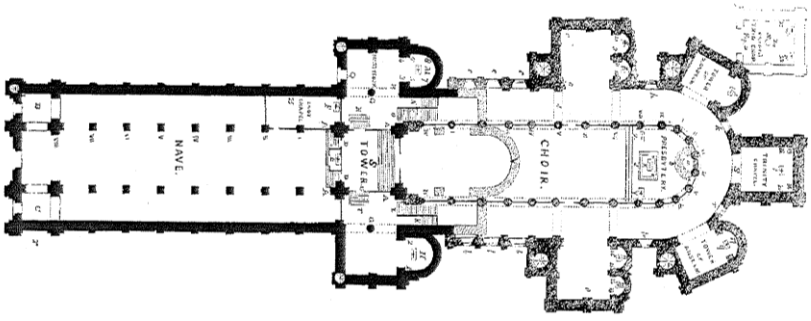

Figure 2-5 Canterbury Cathedral after the reconstruction of the nave in English Gothic style (1390 -1411)

In 1498, the Bell Harry Tower (the tower between the nave and the choir) was extended and the Cathedral was largely complete as seen today. Finally, the original Norman northwest tower was demolished in the late 18th century due to structural concerns (The Canterbury Cathedral Website n.d.). It was replaced during the 1830's with a Perpendicular style twin of the southwest tower, currently known as the 'Arundel Tower'. This was the last major structural alteration to be made to the Cathedral (Figure 2-6). Figure 2-7 presents Canterbury Cathedral in its present condition.

(a) (b)

Figure 2-6 (a) the northwest tower as it was before the demolition - (b) The northwest tower as it looks after its reconstruction in 1830.

Figure 2-7 The Canterbury Cathedral in its present condition

2.2 Conservation and Repair of Canterbury Cathedral after Second World War

2.2.1 1946 – 1968

From 1946 to 1947 one of the Bell Harry pinnacles was finished using Bath stone, a stone which was not compatible with the Caen stone used to construct the medieval cathedral because it was more coarse and grainy in texture and darker in color (Newton 2012).

The walls of Canterbury Cathedral are made of three leaf masonry. Two leaves of masonry, an outer one and an inner one, are made of Caen stone and are bonded together with long tie stones. The intervening gap between these two masonry leaves is filled with a mixture of lime mortar and small fragments of rubble left over the masonry and building works (Newton 2012).

The negative pressure caused by the large bombing during the Second World War is said to have the effect of separating the outer layer of the masonry from the wall. This damage would be very dangerous for the stability of the building and could be become bigger by rain and freezing temperatures (Newton 2012).

In order to restore the initial condition of the masonry, Harold Anderson (Surveyor to the Fabric from 1946 to 1968) inserted a strong Portland cement grout into the masonry for reinstating the integrity of the wall and increasing its strength. Unfortunately, the use of Portland cement had negative consequences for the soft limestone of the masonry by accelerating its decay at the areas where it was used. Anderson also used Bath stone to repair the masonry of Bell Harry Tower (Newton 2012).

2.2.2 1968 – 1991

The architect Peter Marsh succeeded Harold Anderson in 1968 as Surveyor to the Fabric. Peter Marsh tried to find and use again, the imported from northern France, Caen stone but it was impossible to obtain this stone in the desired quantity or quality since the end of the 19th century. Finally, he found another high quality limestone from the south west of France, known as Lepine (Newton 2012).

During his time as surveyor at the Canterbury Cathedral, Peter Marsh undertook the following projects (Newton 2012):

- Rebuilding the gable of the south west transept. He used a reinforced concrete cantilever beam to tie the weight of the gable back into the main structure of the building.
- Conservation of the south window's glass. The glass was put back into the cathedral in specially made brass frames with a layer of protective glazing on the outside.
- Large scale repair works at the west end of the cathedral. Rebuilding the oculus and gable and stone replacements at the south west and north - west towers.

2.2.3 1991 – Present

On 1991 John Burton became the new Surveyor of the Fabric and his most important projects were (Newton 2012):

- Re-flooring of the Cathedral nave, a work that had been started in 1991 and was completed in June 1992. A new Portland concrete slab floor was laid on a lime screed over an under floor heating system, a system which utilized the stone floor as a huge radiator. This work was extended to the south west transept.
- A conservation cleaning program was applied to the original parts of the cathedral by using mild chemical poultices and specialist equipment in order to remove the dark crust that increases the stone's decay and change its color.
- An environmental monitoring system was installed into Canterbury cathedral. The system is gathering information on temperature, relative humidity and movement in the roof spaces, ground floor, crypt, Bell's Harry interior, south west transept and flying buttresses on the south side of the nave.
- Finally, John Burton found a small mine near the French city Caen where the extraction of the "Caen – type" limestone had been re established. Numerous tests confirmed that this stone is similar to the stone used for the construction of the actual cathedral. The first Caen stone block was fixed into reconstructed pinnacles on top of the corona chapel in 2009.

2.3 The Oculus at Canterbury Cathedral

2.3.1 Introduction

Canterbury Cathedral has two ocular windows, called as “eyes”, set in the north wall of the north-east Transept and in the south wall of the south-east Transept (Figure 2-8). The oculi are large Romanesque circular windows that are divided into segments by iron armatures and not by stone tracery as happens with rose windows. There are three reasons that make Canterbury Cathedral’s oculi unique (Vidimus on Line Magazine 2006):

- Early date (1180)
- Large scale (4.47m in diameter)
- Design of the original Ferramenta (the ironwork required to hold the window)

(a) (b)

Figure 2-8 (a) The South Oculus at Canterbury Cathedral - (b) The North Oculus at Canterbury Cathedral

Both oculi of the cathedral are decorated with stained glass panels (Figure 2-9). The North oculus is painted with figures from the Old Testament and retains a large amount of its original stained glass panels. The South Oculus is painted with figures from the New Testament and retain only twelve of the original ornamental panel. The rest of the stained glass panels of the South Oculus were reconstructed by George Austin jnr, the Cathedral glazier from 1848 to 1862 (Vidimus on Line Magazine 2006). Some further details on the South Oculus, which is the subject of this work, follow in this chapter.

(a) (b)

Figure 2-9 (a) The glass of the South Oculus - (b) The glass of the North Oculus

2.3.2 The South Oculus at Canterbury Cathedral

The South Oculus at Canterbury Cathedral is a space frame made from wrought iron which was built between 1178 and 1180. Despite its age, the iron of the Oculus is in remarkably good condition, especially considering the exposure to the environmental conditions[1] (wind and weather) and the structural tribulations of the south gable wall (Geddes 2011). The south oculus consists of one internal and one external layer.

The internal layer is called **Ferramenta** and includes all the ironwork required to hold the window in place. Parts of the Ferramenta are the **armatures** which are the iron frames required to support the glass, have rectangular cross – section and are joined together in neat mortise joints. On the inside of the armature bars, lugs project so that the glass can be pinned in place – and easily removed – with simple wedges (Figure 2-10).

(a) (b)

Figure 2-10 (a) Joint detail of the armatures - (b) System for holding the stained glass on the armatures (Picture of a similar arrangement on another window)

[1] According to George Easton (Cathedral glazier from 1907 to 1971), the chemical analysis of the armatures resulted in a high zinc content, which protects them from corrosion.

The external layer consists of vertical and horizontal bars of round section which create an iron **grille**. The vertical bars are widening at regular intervals so the horizontal bars can pass through them (Figure 2-12a). The horizontal bars are restrained at the intersection with the vertical bars by copper wedges. The joint is then sealed with a lead putty to prevent water ingress (Figure 2-11b).

(a) (b)

Figure 2-11 (a) The iron grille consisting of vertical and horizontal bars of round section - (b) Detail of the copper wedge used in the connection between the bars of the grille

The two iron layers of the Oculus (Ferramenta and Grille) are connected to each other by over fifty iron rods, the pins (Figure 2-12a). The end of the pin connected to the grille has the form of a circular eye and is fixed to the bars by using copper wedges. Also in this case the joint is then sealed with lead putty to prevent water ingress. The other end of the pin passes through a hole in the armature and then is hammered flat, like a cold rivet (Geddes 2011). The length of these metal rods varies between 130 and 150 mm, which is also the distance between the two layers of the space frame.

The space frame is fixed into the masonry as Figure 2-12b shows.

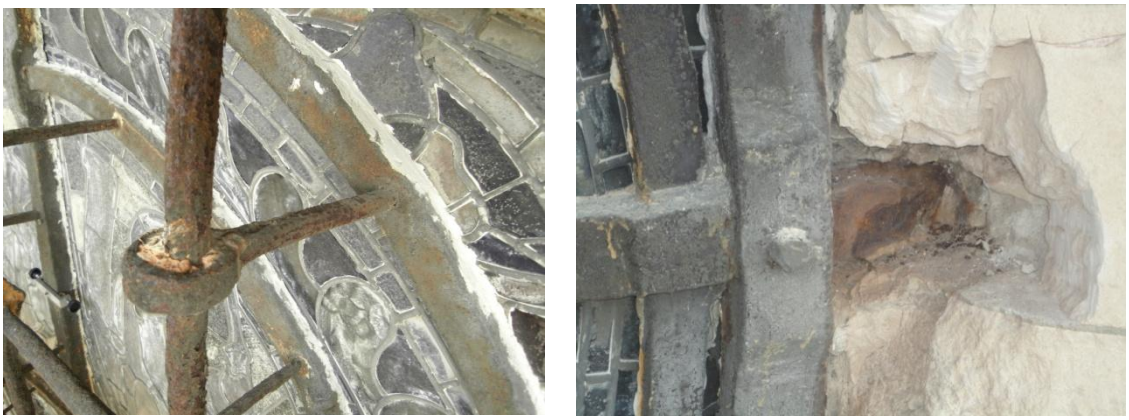

Figure 2-12 (a) Detail of an iron pin which connects the two layers of the space frame, (b) Fixing of the space frame into the masonry

The two - layer structural system of the South Oculus is almost certainly the original construction (around 1180), as scars on the outside of the North Oculus Ferramenta roughly correspond with the rod attachments on the South Oculus, indicating that a similar reinforcement was originally in place on the north side (Vidimus on Line Magazine 2006). Figure 2-13 shows the comparison between the South and North Oculus related to the Ferramenta – Grille fixing points.

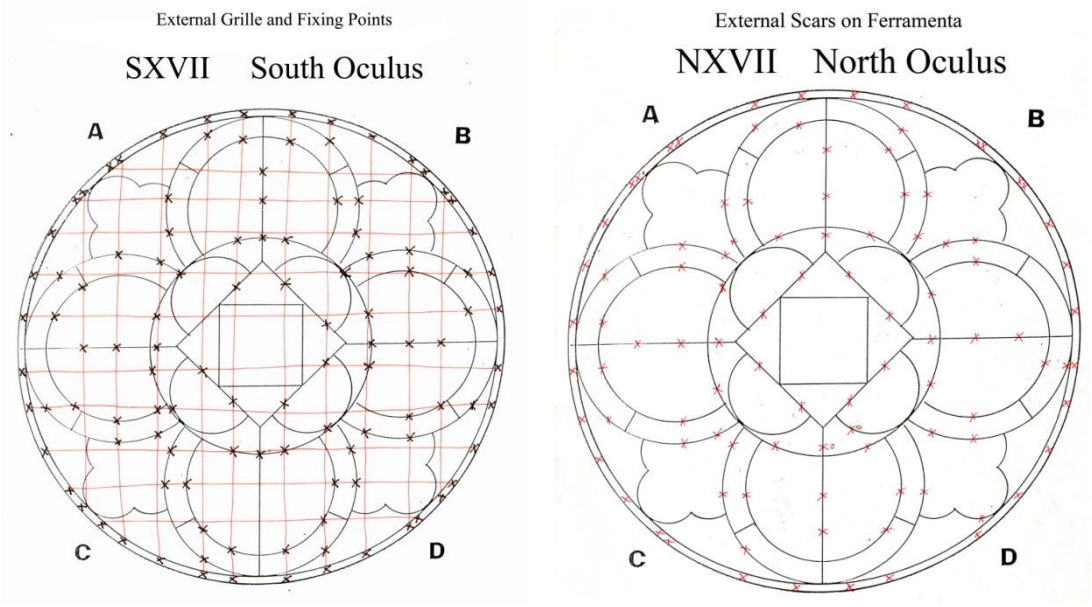

(a) (b)

Figure 2-13 Fixing points between the Ferramenta and the grille: (a) South Oculus - (b) North Oculus

3. SURVEY AND NON – DESTRUCTIVE TESTS

Introduction

This chapter presents the results of the experimental campaign, which took place at the South Oculus at Canterbury Cathedral from 19 to 21 April 2011, carried out from the structural department of Minho University, Portugal. The aim of this campaign was to collect information on the geometry and condition of the structural members and to estimate the dynamic response of the oculus by an Ambiental Vibration Testing.

3.1 Survey of the Ferramenta

In general, the Ferramenta members were in very good condition despite their 850 years age, as no remarkable change in their initial shape was noticed and damage was limited.

3.1.1 Deterioration and damage

Except for one broken section, no damage was noticed in the Ferramenta members (Figure 3-1a). There are a number of old repairs but they do not seem to affect the stability of the structure (Figure 3-1b). Moreover, there is a coating of corrosion products on the iron's surface, but considering the environmental exposure and age, this corrosion level is considered low.

(a) (b)

Figure 3-1 (a) Broken Ferramenta section – (b) Old repair at the Ferramenta circular ring

3.1.2 Connections

The connections of the Ferramenta members are made using “mortise and tenon” joints by preheating the member with the mortise and are in very good condition. They will therefore be considered as rigid connections later in this work (Figure 3-2).

Figure 3-2 Detail of the connections condition in Ferramenta

3.1.3 Sections

The sections of the Ferramenta members are of rectangular shape and were measured using a digital caliper (Figure 3-3). One measurement has been made for each member due to the limited time available to carry out the survey.

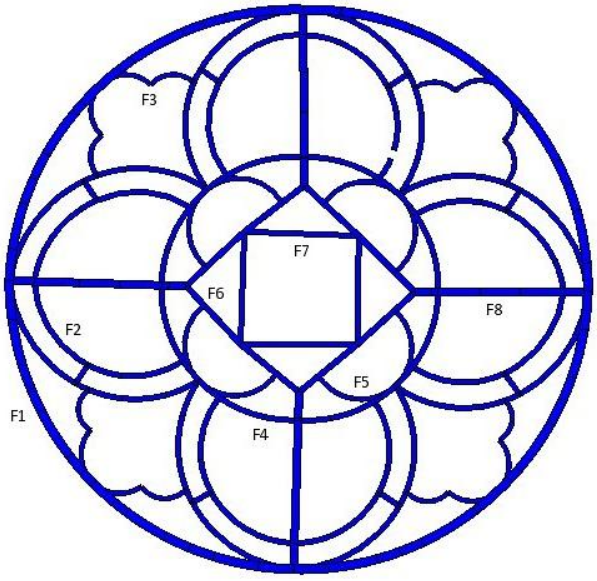

Section	Width x Thickness [cm]
F1	7.0x5.0
F2	4.0x2.7
F3	3.5x2.7
F4	4.5x3.5
F5	3.5X3.0
F6	4.5x3.5
F7	4.0x3.0
F8	6.0x4.0

Figure 3-3 Sections of the Ferramenta members and locations of the measurements taken

3.2 Survey of the Grille

The inspection at the grille has revealed that it has been more affected by the passage of time. In particular, because of the deformation of the horizontal and vertical iron bars, the grille does not have a regular spacing of bars anymore and there is significant curvature. It is also possible that part of the above deformation was introduced at the moment of installing the window and was caused by misalignments which seem very likely to occur for such a big structure (Figure 3-4).

Figure 3-4 Curvature of the Horizontal and Vertical grille bars

3.2.1 Deterioration and damage

The third vertical grille bar from the left is broken (Figure 3-5a), whereas some bars were repaired by using tube sections (Figure 3-5b). These loose tubes should be removed as they are promoting corrosion to the iron grille (Hall 2011). Furthermore, the shape of the bars is not perfectly circular due to their exposure to the elements for so many centuries.

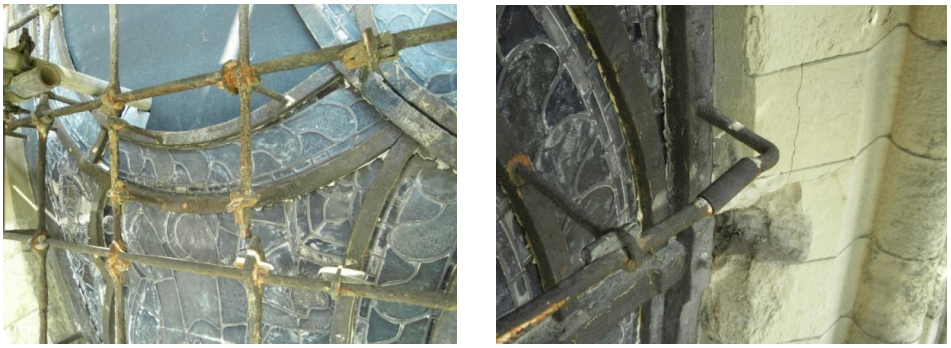

(a) (b)

Figure 3-5 (a) Detail of the broken vertical grille bar – (b) Bar repaired using tube section

3.2.2 Connections

The horizontal bars are passing through the vertical bars and they are joined together by using copper wedges and lead putty (Figure 3-6). We will see later in this work that these connections of the grille will not be considered rigid, but semi – rigid. The grille connections are in very good condition and no loss of material can be observed. In addition, the presence of dissimilar materials at the grille joints (wrought iron, copper and putty) could cause electrochemical (galvanic) corrosion, which seems not to be occurring (Hall 2011).

Figure 3-6 Detail of the grille bars connections

3.2.3 Sections

The sections of the grille bars were measured using a digital caliper. Two readings were taken for each bar, one in the vertical and one in the horizontal direction, as being the bars deteriorated with not perfectly circular sections. Figure 3-7 and Table 3-1 present the data of the measurement. Again, only one measurement has been taken for each section due to the limited time available to carry out the survey.

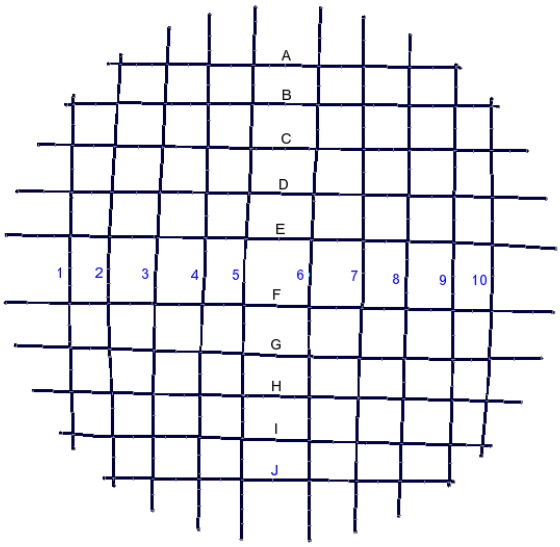

Figure 3-7 Identification of the grille bars

Table 3-1 Sections of the grille bars [mm]

	Horizontal Bars				Vertical Bars		
	S_1	S_2	S_{avg}		S_1	S_2	S_{avg}
A	22.25	25.25	23.75	**1**	21.5	23.2	22.35
B	22.5	21.6	22.05	**2**	21.1	23.7	22.4
C	24.75	22.5	23.625	**3**	24.75	27.7	26.225
D	25.7	25.1	25.4	**4**	20.9	24.6	22.75
E	26.05	25.15	25.6	**5**	21.9	24.9	23.4
F	26.8	25.15	25.975	**6**	23.8	28.6	26.2
G	25.85	23.9	24.875	**7**	23.45	26.8	25.125
H	24.02	21.7	22.86	**8**	22.7	24.4	23.55
I	24.9	23.85	24.375	**9**	21.1	23.4	22.25
J	24.8	23.8	24.3	**10**	22.9	25.5	24.2
Average			**24.281**				**23.845**

3.3 Survey on the Pins

The majority of the pins have a similar shape, with the exception of the hardly deteriorated pins whose original geometry is lost and the new pins that replaced the failed pins (Figure 3-8).

(a) (b) (c)

Figure 3-8 (a) Typical old pin – (b) New pin – (c) Hooked pin with severe deterioration

3.3.1 Deterioration and damage

The inspection showed that the pins are the most deteriorated part of the structure. Scars on the Ferramenta reveal that many of the original pins are missing from the structure. Moreover, the majority of the pins have suffered serious reduction of their section near the connection with the Ferramenta, making them a weak point for the structure. In some cases this reduction is up to 50 %. Furthermore, the “eye” of many pins is totally destroyed, making them inactive (Figure 3-9). This is because the electrochemical reactions between the wrought iron pins and the wrought iron grille and ferramenta, created corrosion (Hall 2011).

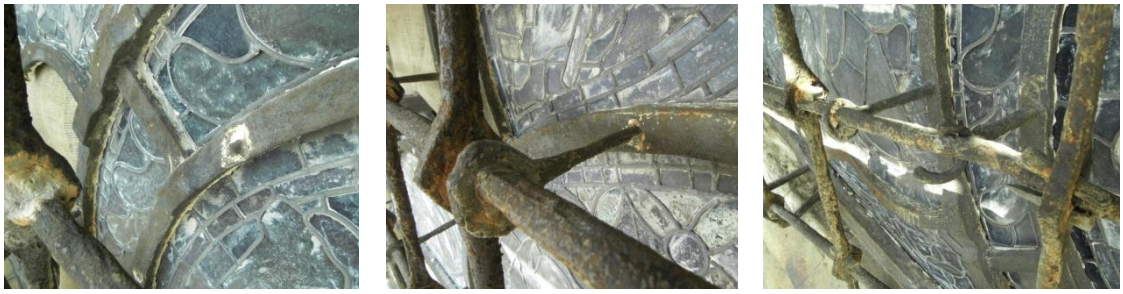

(a) (b) (c)

Figure 3-9 (a) Missing pin – (b) Reduced pin section close to the ferramenta – (c) Broken pin “eye”

3.3.2 Connections

The connections of the pins to the Ferramenta (cold rivets) are in good condition and will be assumed as rigid later in this work. On the contrary, the pins are joined to the grille bars by using copper wedges and lead putty. This type of connection will be considered as semi – rigid. The grille - pin joints were inspected one by one and two types of failure were identified (Figure 3-10):

1. Destroyed pin “eye” because of the deterioration
2. Loss of wedges and putty

(a) (b)

Figure 3-10 (a) Type of Failure 1 – (b) Type of Failure 2

Figure 3-11 presents the classification of the pins as active (green) or inactive (red). According to the inspection 9 pins were classified as inactive.

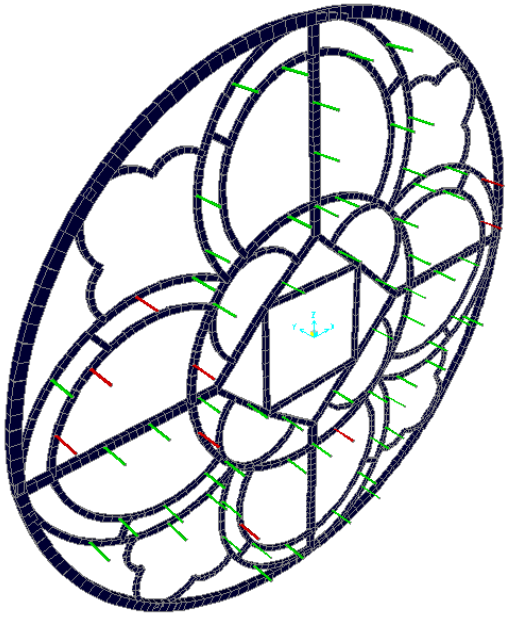

Figure 3-11 Classification of the pin sections as active (green) or inactive (red)

3.3.3 Sections

As addressed before, the sections of the pins are not constant. For this reason the diameter of each pin was measured at three points along its axis, with the digital caliper (Figure 3-12). Two measurements were taken at each point, one horizontal and one vertical. Note that forty - five pin sections (out of total of seventy one) were measured due to the limited time available to carry out the survey. Table 3-2 presents the range of average values measured at each point.

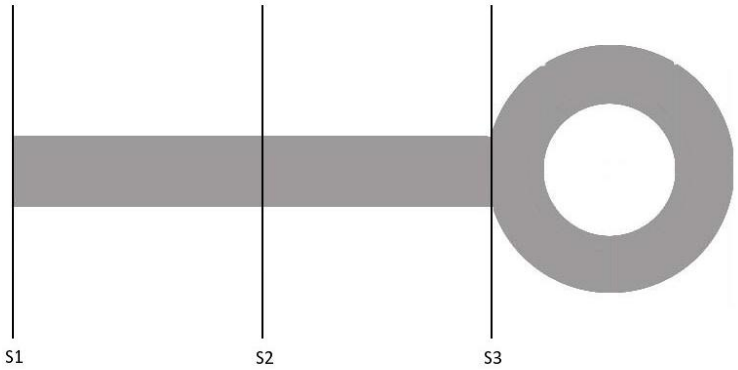

Figure 3-12 Drawing of the measured points along the axis of each pin

Table 3-2 Range of the average diameter values measured at the sections S1, S2 and S3 of the pins

$S1_{avg}$ [mm]		$S2_{avg}$ [mm]		$S3_{avg}$ [mm]	
Min	**Max**	**Min**	**Max**	**Min**	**Max**
8.74	21.27	12.11	20.21	13.05	21.14

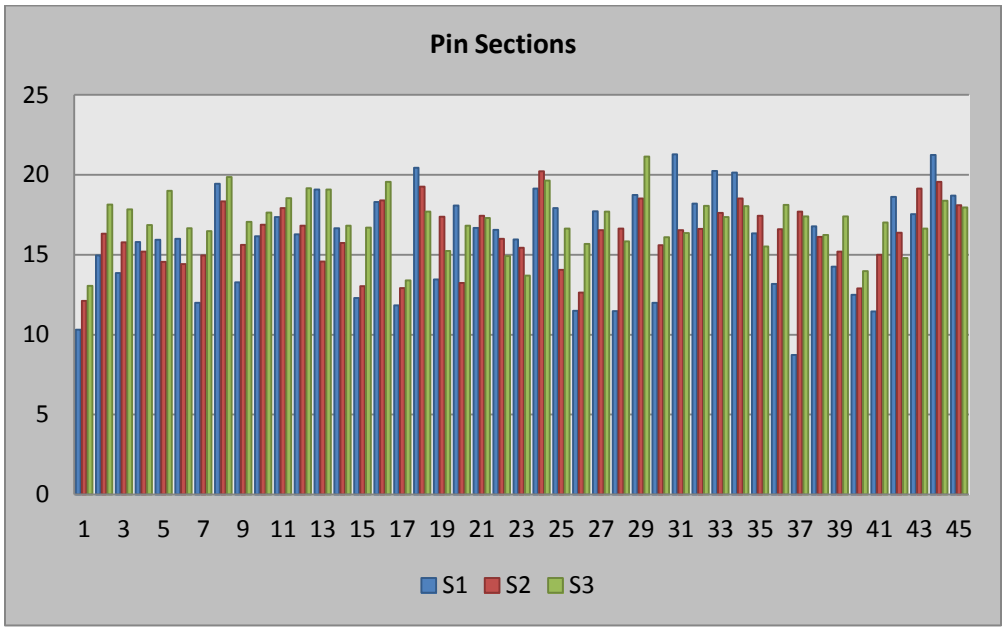

Figure 3-13 Summary of the measurements at the pins

Figure 3-13 presents the summary of the measurements of the pins. According to that, the pins were classified into two groups (Figure 3-14), Type 1 and Type 2, according to the following procedure:

Type 1

- Pins with $S1_{avg}$ diameter greater than 15 mm ($S1_{avg} \geq 15mm$)
- The section is assumed constant with $d = (S1_{avg}+S2_{avg}+S3_{avg})/3$

Type 2

- Pins with $S1_{avg}$ diameter smaller than 15 mm ($S1_{avg} < 15mm$)
- The section is divided in one deteriorated part, with $d = S1_{avg}$, and in one non - deteriorated part, with $d = (S2_{avg}+S3_{avg})/2$

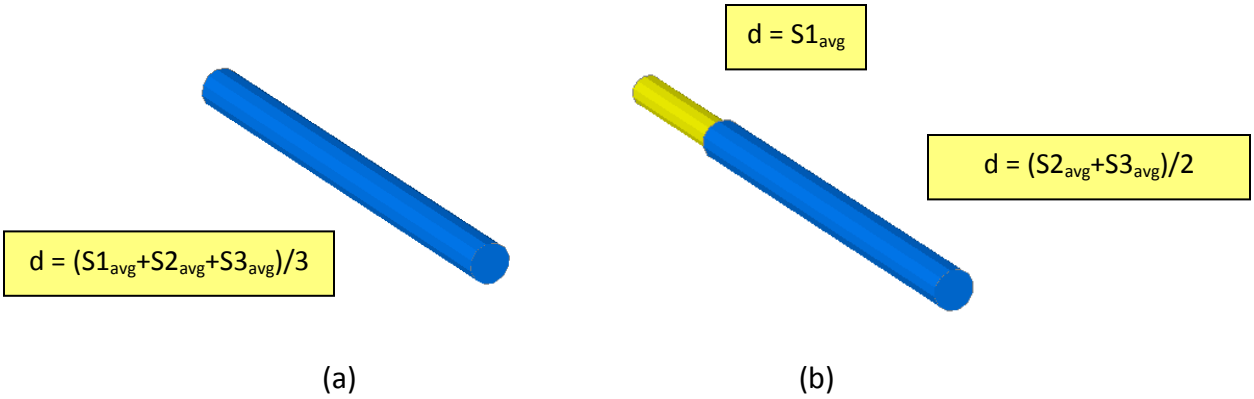

Figure 3-14 (a) Type 1 pin sections – (b) Type 2 pin sections

3.4 Survey on the Surrounding Masonry

3.4.1 Anchor Points

Close examination of the surrounding masonry revealed that the Oculus is restrained into the masonry at 16 anchor points (Figure 3-15).

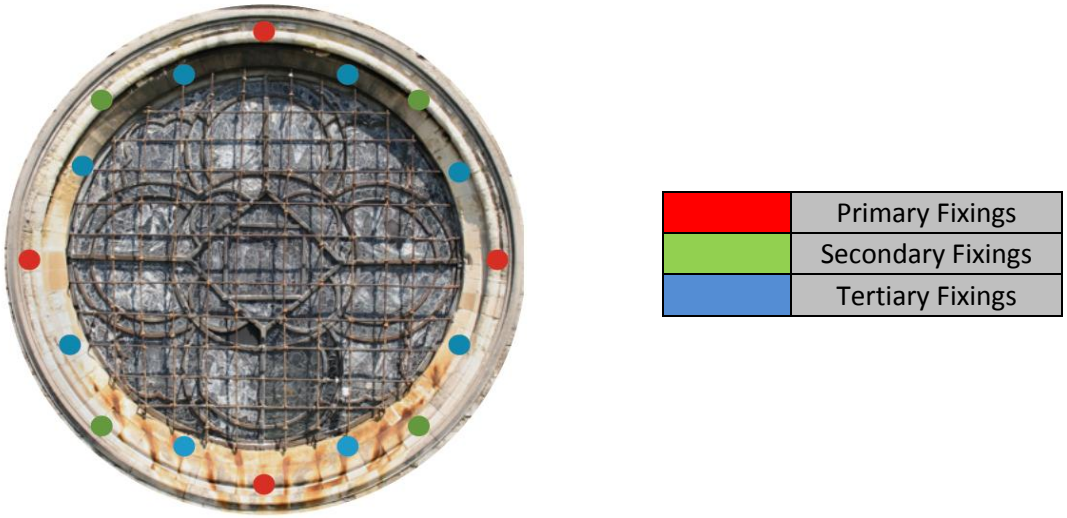

Figure 3-15 Anchor points of the Oculus into the masonry (Hall 2011)

3.4.2 Deterioration and damage

In general, the masonry is in very good condition except the anchor point at three o' clock where stone detachment can be noticed (Figure 3-16). This damage is from rust jacking of the iron fixings promoted by water ingress to the stone through failed pointing and joints (Hall 2011).

Figure 3-16 Stone detachment at anchor point (picture taken after local opening up)

3.5 Ambiental Vibration Test

3.5.1 State of the art

Modal identification or dynamic identification analysis is a procedure that combines vibration testing techniques and analytical methods to determine modal parameters of structures such as frequencies, mode shapes and damping coefficients.

In order to estimate the dynamic parameters, the structures can be excited with ambient (natural) vibrations, such as the wind load, traffic or even human's induced vibrations, or forced vibrations such as drop weights, eccentric mass excitators or other. When ambient vibration is used, the process is called output – only modal identification which means that the modal analysis is carried out without knowing and/or controlling the input excitation. In this way, the excitation is considered a white noise signal and only the structural response is measured with highly sensitive sensors.

3.5.2 Preliminary Numerical Results

In order to plan the ambiental vibration test it was necessary to estimate, before the experimental campaign, the dynamic behavior of the structure (eigen modes, eigen frequencies). For that reason, a preliminary numerical model was built in the finite element software SAP2000 (SAP2000 User's Manual Release 14.1.0). Literature values were assumed for the mechanical and physical properties of the material (Bussell 1997) and the cross sections of the structure's components were considered as constant, according to the drawings provided by Claudio Corallo of the Morton Partnership LTD. Figure 3-17 and Table 3-3 present the results of the Eigen value analysis.

Table 3-3 Eigen Frequencies

Mode	1	2	3	4	5	6	7	8	9	10
Frequency [Hz]	11.64	19.31	19.85	29.00	34.53	37.62	40.50	41.50	49.44	49.87

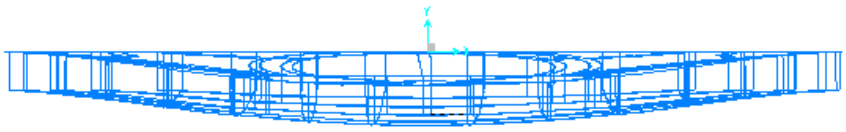

Mode 1 (f=11.64 Hz)

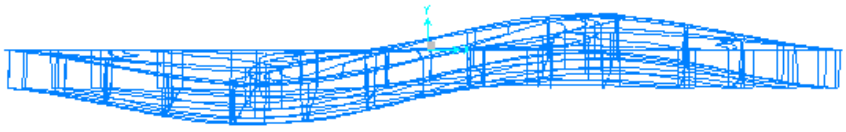

Mode 2 (f=19.31 Hz)

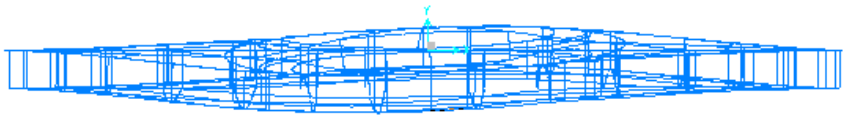

Mode 3 (f=19.85 Hz)

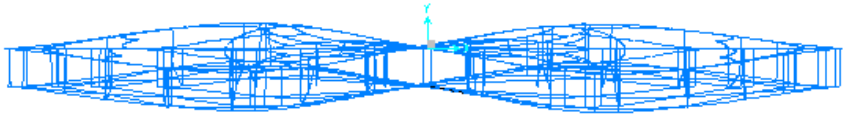

Mode 4 (f=29.00 Hz)

Figure 3-17 Numerical mode shapes.

3.5.3 Test Planning

In the dynamic identification of the Oculus, performed by University of Minho, an acquisition chain composed by four piezoelectric accelerometers, with bandwidth ranging from 0.15 to 1000 Hz, dynamic range ± 0.5 g and a sensitivity of 10 V/g, connected to a data acquisition system with 24-bit resolution was used (Figure 3-18).

(a) (b)

Figure 3-18 Measuring equipment: (a) data acquisition, (b) accelerometer

To measure the dynamic response of the Oculus to ambient vibrations, 18 points of the structure were selected. The accelerometers were fixed on the ferramenta and grille, in the orthogonal direction to the Oculus. As the experimental tests were based on the measurement of ambient vibration with sequential data sets (setups), two points (one on grille and another on the Ferramenta) were selected to be reference points (Figure 3-19)

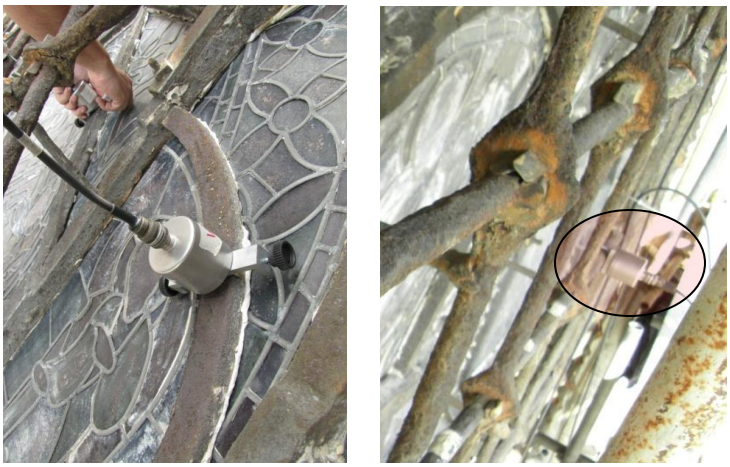

(a) (b)

Figure 3-19 Reference measuring points: (a) Ferramenta, (b) Grille

The measuring points were chosen in order to identity the dynamic behaviour of the grille and ferramenta, as well as to evaluate the degree of connection between these two layers. The ambient vibrations were measured in all of the 18 points with 14 sequential setups, with a sampling frequency of 200 Hz and a total sampling of 10 min. In the first two setups four accelerometers were used. However, due to a technical problem in following setups only three accelerometers were used.

Output-only modal identification technique was used to estimate the modal parameters: resonant frequencies, mode shapes and damping coefficients. This technique is based on the dynamic measurements of a virtual system under natural (ambient or operational) conditions, and it is based on the assumption that the excitation is reasonably random in time and in the physical space of the structure (Ewins 2000), (Brincker, Zhang and Andresen 2000). In the case of the Oculus, the ambient vibrations were mainly induced by the wind.

3.5.4 Experimental Results

The Unweight Principal Component (UPC) technique, implemented in the software ARTeMIS Extractor Pro (ARTeMIS User's Manual Release 5.3), was used to estimate the dynamic parameters. This technique operates in the time domain and is based on the Stochastic Sub-space Identification (SSI) method. The UPC was selected because it is robust and allows modal parameters estimation with high frequency resolution (Peeters 2000).

The maximum amplitude of vibration was lower than 6 mg and the time history are randomly in time (Figure 3-20). In Figure 3-21 it is possible to observe four stable modes in the frequency range under 17 Hz, while it is difficult to specify a stable mode over the frequency of 17 Hz. In overall, 10 modes were estimated.

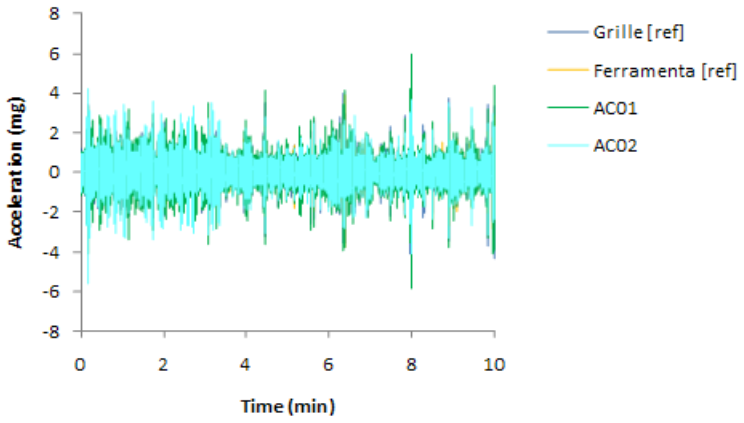

Figure 3-20 Signals of Setup 1

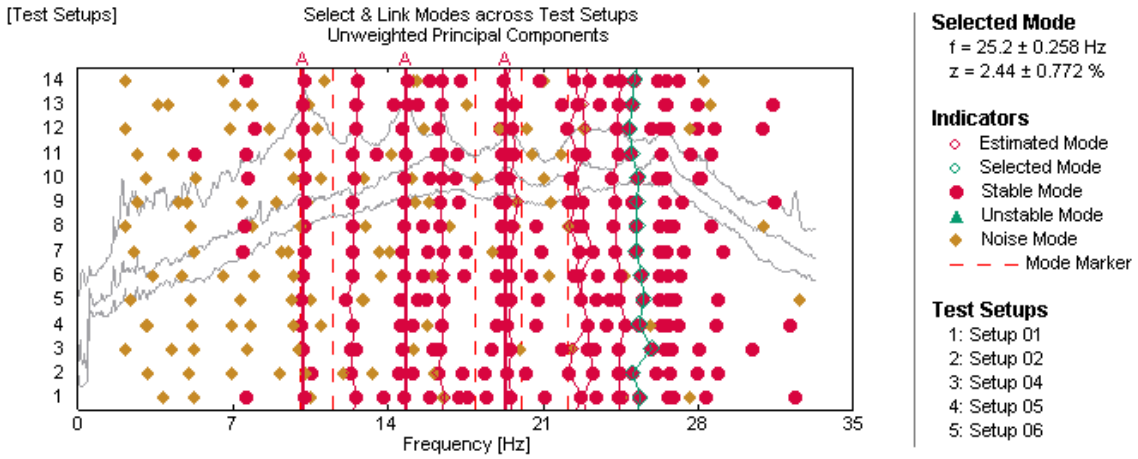

Figure 3-21 Model selected for select and link modes across test setups

Table 3-4 summarizes the experimental values for the 10 modes estimated through UPC method. From the comparison with the preliminary numerical results it is obvious that the range of the numerical frequencies (11.64 Hz – 48.87 Hz) is much wider than the range of the experimental frequencies (10.23 Hz – 25.25 Hz). That means that the real structure is more flexible than the preliminary finite element model. Table 3-4 also shows that the experimental modes 5 – 6, 7 – 8 and 9 – 10 have very similar frequencies.

Table 3-4 Frequency and damping coefficient of the first 10 experimental modes

Mode	Experimental Frequency [Hz]	Experimental Damping [%]	Numerical Frequency [Hz]
1	10.23	2.60	11.64
2	12.85	2.55	19.31
3	14.77	1.80	19.85
4	16.51	2.00	29.00
5	19.19	2.42	34.53
6	19.80	2.41	37.62
7	22.58	3.25	40.50
8	22.68	3.23	41.50
9	24.84	1.74	49.44
10	25.25	3.31	49.87

Figure 3-22 and Figure 3-23 present the 10 experimental mode shapes as they were estimated through UPC method. The first six modes are global with a regular shape and have single or double curvature (Figure 3-22), while the shape of the higher modes is very complex (Figure 3-23).

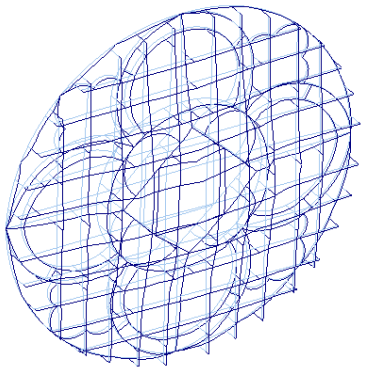

Mode 1

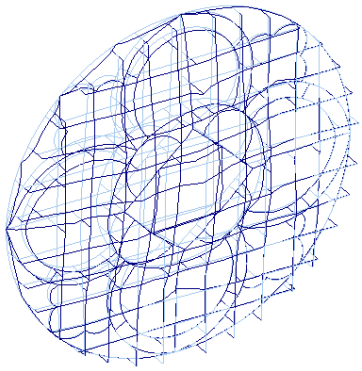

Mode 2

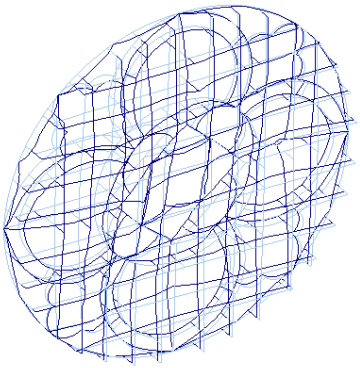

Mode 3

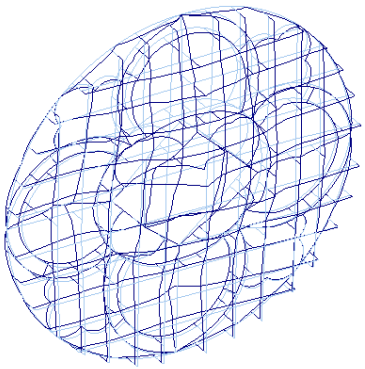

Mode 4

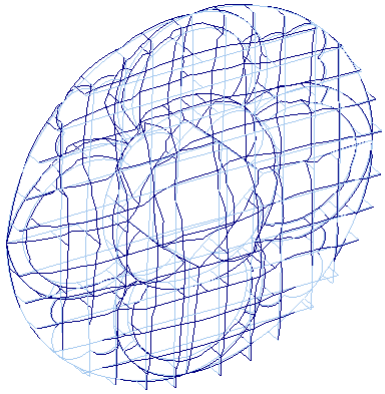

Mode 5

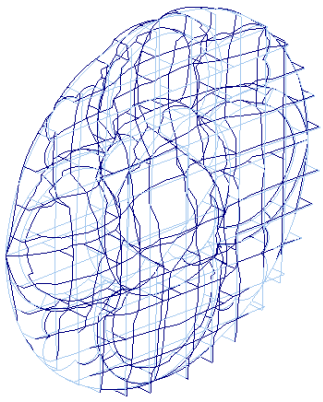

Mode 6

Figure 3-22 Experimental mode shapes 1 – 6

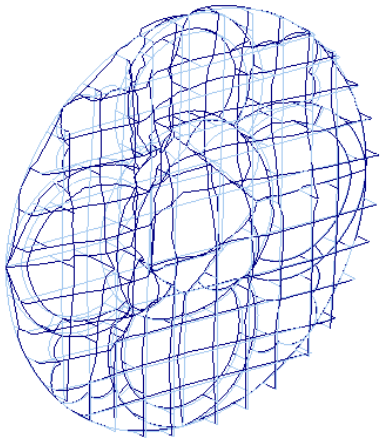

Mode 7

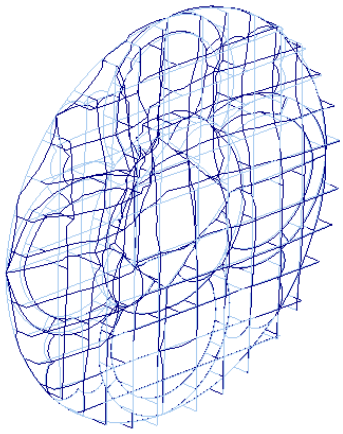

Mode 8

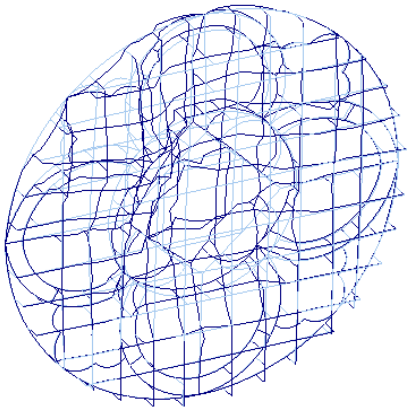

Mode 9

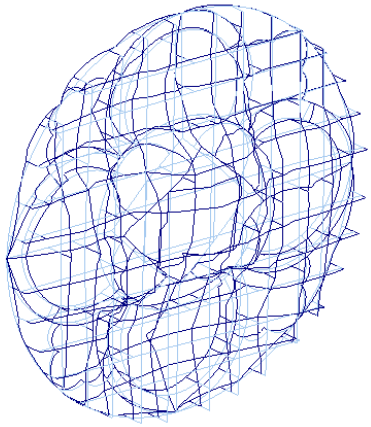

Mode 10

Figure 3-23 Experimental mode shapes 7 – 10

4. MODEL UPDATING

Introduction

This chapter describes the procedure followed in order to calibrate the Finite Element Model of Canterbury Cathedral's South Oculus, according to the experimental results of the ambiental vibration test. This was a difficult and time consuming procedure as being the south Oculus a very old wrought iron structure. The geometry is irregular, some connections are not rigid and also the importance of the structure does not allow taking any specimen for testing the mechanical and physical properties of the material. Thus six different types of models were built in the Finite Element Software, DIANA (DIANA User's Manual Release 9.4), and the results of the Eigenvalue analysis have been compared with the experimental data in order to achieve the most realistic finite element model.

4.1 General information on the Finite Element Model

4.1.1 Geometry

The Oculus model was firstly simulated in the CAD software, AutoCAD 2010 (Autocad User's Manual Release 2010) and then it was inputted into the Finite Element software, DIANA. As Figure 4-1 shows, the model contains only bar elements representing the Ferramenta, the Pin and the Grille members, in a 3-D arrangement. The finite element model does not contain 2-D members for the simulation of the stained glass.

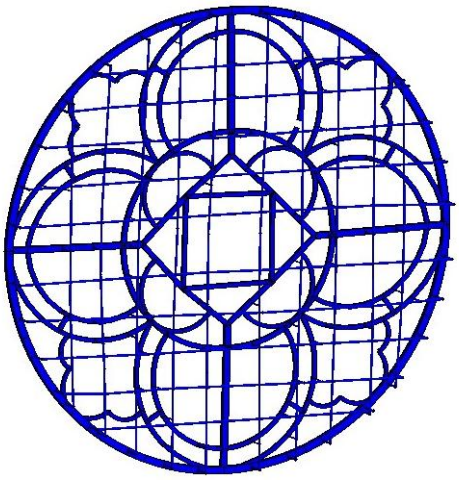

Figure 4-1 Finite Element model of the Oculus of the Canterbury Cathedral

4.1.2 Finite Element Meshing

In all the finite element models used during the calibration procedure, the bar members of the Ferramenta, Pins and Grille were meshed using the three - node curved beam element **CL18B** from the iDIANA element library. The CL18B element is a three – node, three dimensional class III beam element (Figure 4-2). Basic variables are the translations u_x , u_y and u_z and the rotations ϕ_x, ϕ_y and ϕ_z (Figure 4-2).

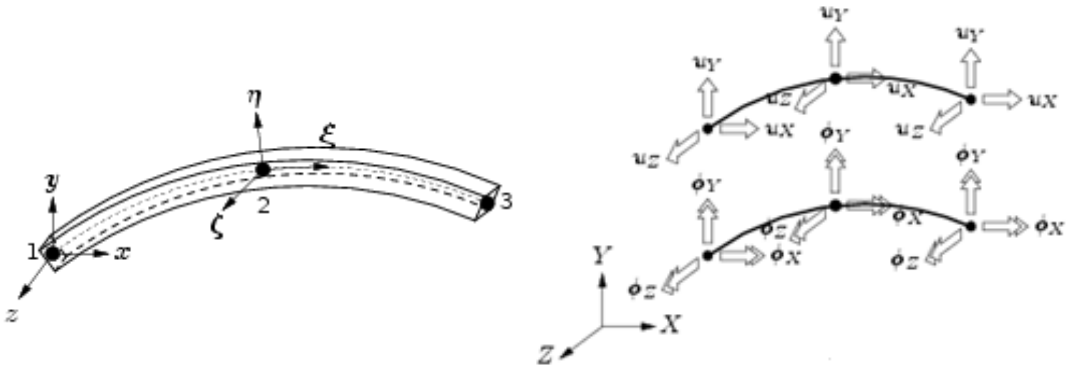

(a) (b)

Figure 4-2 The CL18B curved three node beam element. (a) Local and global axes, - (b) Displacements for the class III beam elements

The interpolation polynomials for the displacements and rotations can be expressed as:

$$u_i(\xi) = \alpha_{i0} + \alpha_{i1}\xi + \alpha_{i2}\xi^2$$
$$\phi_i(\xi) = b_{i0} + b_{i1}\xi + b_{i2}\xi^2$$

4-1

Due to these polynomials the strains vary linearly along the center line of the beam. The primary strains of the three-dimensional class-III elements are the Green-Lagrange strains:

$$\varepsilon = [\varepsilon_{xx}\ \gamma_{xy}\ \gamma_{zx}]^T$$

4-2

The primary stresses are:

$$\sigma = [\sigma_{xx}\ \sigma_{xy}\ \sigma_{zx}]^T$$

4-3

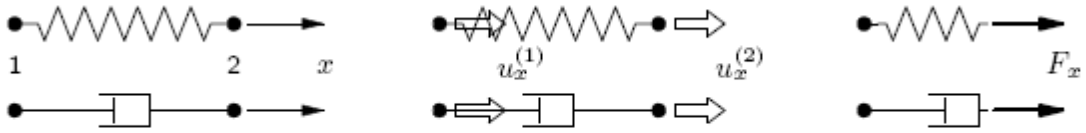

(a) topology (b) displacement (c) stress

Figure 4-3 The SP2TR two - node spring element

In the finite element models where springs were used to simulate the semi – rigid connection between a) Pins – Grille bars and b) Horizontal – Vertical Grille bars, **SP2TR** were the selected spring element from the elements library of DIANA. The SP2TR element (Figure 4-3) is a two – node translation spring/dashpot. Basic variables of the SP2TR element are the translations, the elongation and the axial force. No time dependency behavior (dashpot) is used here.

$$u_e = [u_x] \qquad \varepsilon = [\Delta u_x] \qquad \sigma = [F_x]$$

4-4

4.1.3 Boundary Conditions

In all the finite element models, it was assumed that the Oculus is fixed into the masonry wall at 16 points (Figure 4-4). All the translational and rotational degrees of freedom at these nodes were fully restrained.

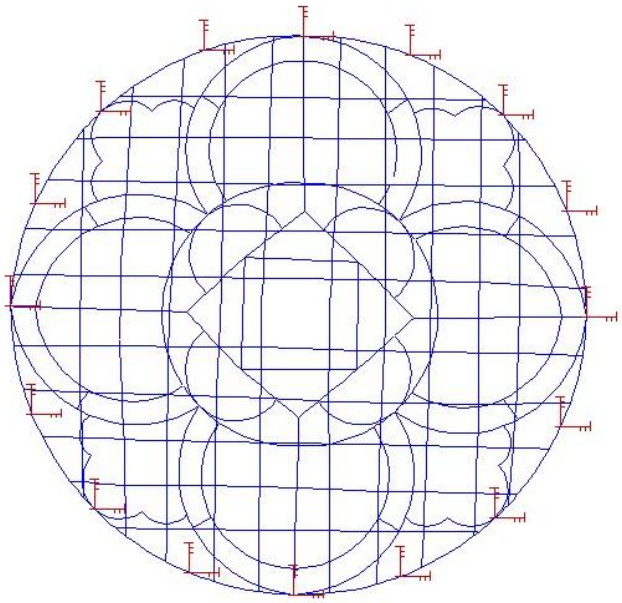

Figure 4-4 Restraint points of the finite element model

4.1.4 Section Properties

Figure 4-5 and Figure 4-6 show the cross sections used for the Ferramenta rectangular members and the Grille bars respectively, in all the finite element models during the calibration procedure, see also chapter 3.

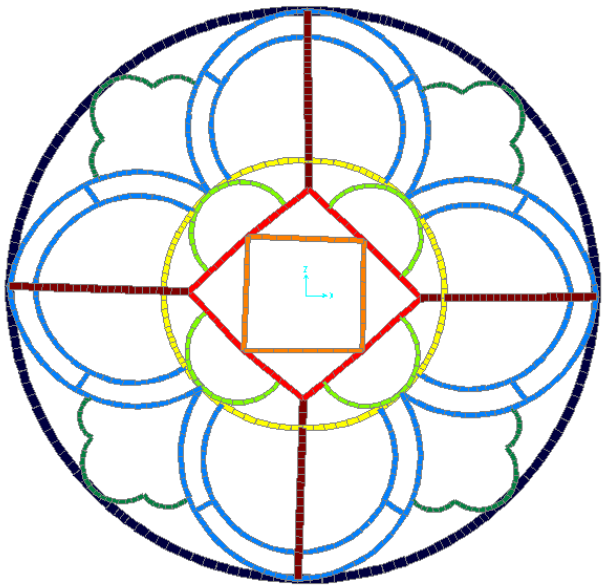

Section	Color	Width x Thickness [mm]
F1		70x50
F2		40x27
F3		35x27
F4		45x35
F5		35X30
F6		45x35
F7		40x30
F8		60x40

Figure 4-5 Cross section index of the Ferramenta members

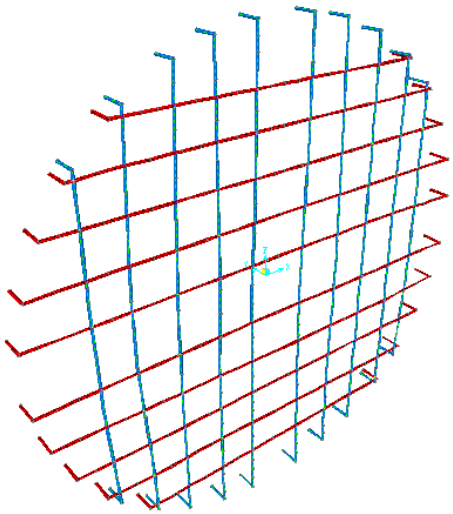

Section	Color	Diameter [mm]
G1		24
G2		24

Figure 4-6 Cross sections of the grille bars

As mentioned in Chapter 3, the majority of the Pins connecting the Ferramenta and the Grille are seriously deteriorated. Because of that reason, the cross sections of the pins are not constant along their length and some necking can be observed at the connection with Ferramenta. Two types of Pin sections were considered into the calibration finite element models (Figure 4-7):

1. Non deteriorated pins with constant section, having diameter d=15 mm (Type A)
2. Deteriorated pins with sections classified according to the procedure presented in Chapter 3 (Type B)

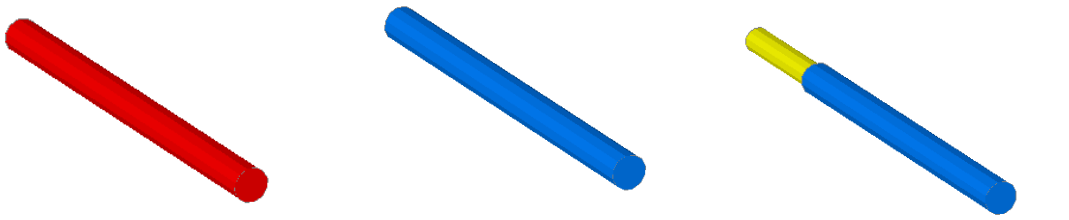

Type A (d=15 cm) Type B (d_{min}≥15 mm) Type B (d_{min}≤15 mm)

Figure 4-7 Pin sections

4.1.5 Material Properties

The mechanical and physical properties of the wrought iron used in all the analysis models have been obtained from the literature (Table 4-1) (Bussell 1997).

Table 4-1 Material Properties

Material	Density, ρ [kgr/m^3]	Young's modulus, E [GPa]	Poisson ratio, v
Wrought iron	7750	154 - 220	0.25

4.1.6 Mass Source

In all the Eigenvalue analyses carried out during the calibration procedure, the only mass considered was that of the wrought iron members of the structure, using the density given in the previous section.

4.2 Calibration Model 1 (CCF1)

4.2.1 Eigenvalue Analysis Data

In this first calibration model, it is assumed that the structure is in ideal condition, i.e. the connections of the Ferramenta, Grille and Pin members were considered rigid, while no damage was taken into account in the structure. This is a simplistic arrangement that will be refined in the following analyses. The finite element mesh contains 2129 nodes and 1184 elements. Table 4-2 contains a summary of the analysis data.

Table 4-2 Eigenvalue analysis data

CCF1	Connections	Damage	Sections	E [GPa]	ν	ρ [kgr/m^3]
Ferramenta	Rigid	No	Constant	185	0.25	7750
Grille	Rigid	No	Constant	185	0.25	7750
Pins	Rigid	No	Type A	185	0.25	7750

4.2.2 Eigen Frequencies

The eigenvalue analysis was executed in Diana and the first ten modes are presented in Table 4-3, in terms of frequency. By comparing the experimental with the numerical results, it is obvious that the numerical model is much stiffer than the experimental one, with the exception of the first mode. Moreover, all the modes have a very low modal participation mass ratio (Table 4-3), except of the first mode which participates in the oscillation with 45.17% of the total mass. This also means that the most important mode of the structure is the first.

Table 4-3 Comparison of the experimental and numerical results

	Experimental	Numerical	
Mode	**Artemis [Hz]**	**Diana - CCF1 [Hz]**	**Modal Participation Mass [%]**
1	10.23	10.20	45.17
2	12.85	17.70	0.00220
3	14.77	18.10	0.00045
4	16.51	26.00	0.00062
5	19.19	33.00	1.33
6	19.80	35.00	7.97
7	22.58	37.90	0.026
8	22.68	38.80	0.011
9	24.84	46.00	0.0011
10	25.25	46.40	0.000017

4.2.3 Correlation of the Mode Shapes (MAC)

The comparison of the Eigen frequencies of two scenarios, e.g. experimental and numerical results, is not enough, and also the mode shapes should be compared. The most well known procedure to study the numerical correlation between two sets of mode shape vectors is to use the Modal Assurance Criteria (MAC) value (Ramos 2007), given by:

$$MAC_{u,d} = \frac{\left| \sum_{i=1}^{n} \varphi_i^u \, \varphi_i^d \right|^2}{\sum_{i=1}^{n} \left(\varphi_i^u\right)^2 \sum_{i=1}^{n} \left(\varphi_i^d\right)^2}$$

4-5

Here ϕ^u and ϕ^d are the mode shape vectors for the two different stage conditions and n indicates the number of estimated degrees of freedom. The expression leads to a scalar value between zero and one, associated with low and high correlation between the two vectors (Ramos 2007).

Table 4-4 presents the correspondent experimental mode shapes to the first three numerical, as they correlated according to the Modal Assurance Criteria (MAC). For the three pairs of modes, the calculated MAC values are considered low. Especially, for the first numerical mode which is the most important, the MAC value 0.81 is hardly acceptable.

Table 4-4 Correlation between experimental and numerical mode shapes

Experimental		Numerical			
Mode	**Artemis [Hz]**	**Mode**	**Diana [Hz]**	**Difference [%]**	**MAC**
1	10.23	**1**	10.20	0.29	0.808
8	22.68	**2**	17.70	21.96	0.332
3	19.19	**3**	18.10	5.68	0.607

4.2.4 Calibration Result

The calibration model **CCF1** is not accepted as the final model because:

- It is much stiffer than the real structure, as the eigen frequency range shows.
- The MAC values for the first three numerical modes are low.
- It does not correspond to the real condition of the structure since no damage was considered.

4.3 Calibration Model 2 (CCF2)

4.3.1 Eigenvalue Analysis Data

In this second calibration model of the Oculus, damage is added into the structure. Specifically, nine broken pins, one broken section of the Ferramenta and one broken section of the Grille were introduced (Figure 4-8). The connections of the Ferramenta, Grille and Pin members were considered rigid. The finite element mesh contains 2126 nodes and 1177 elements.

Table 4-5 contains a summary of the analysis data.

Figure 4-8 Damage imported into the finite element model CCF2

Table 4-5 Eigenvalue analysis data

CCF2	Connections	Damage	Sections	E [GPa]	ν	ρ [kgr/m^3]
Ferramenta	Rigid	Yes	Constant	185	0.25	7750
Grille	Rigid	Yes	Constant	185	0.25	7750
Pins	Rigid	Yes	Type A	185	0.25	7750

4.3.2 Eigen Frequencies

The eigenvalue analysis was executed in Diana and the first ten modes are presented in Table 4-6, in terms of frequency. By comparing the experimental with the numerical results it can be said that after the damage is imported into the model, the numerical model is more flexible than CCF1, but it remains much stiffer than the experimental one in all the modes except the first, where the numerical model is more flexible. Moreover, all the modes have a very low modal participation mass ratio (Table 4-6) except of the first mode which participates in the oscillation with 44.5% of the total mass.

Table 4-6 Comparison of the experimental and numerical results

	Experimental	Numerical	
Mode	**Artemis [Hz]**	**Diana – CCF2 [Hz]**	**Modal Participation Mass [%]**
1	10.23	9.91	44.52
2	12.85	17.3	0.023
3	14.77	17.8	0.0045
4	16.51	25.3	0.0047
5	19.19	32.1	2.71
6	19.80	34.0	6.50
7	22.58	36.4	0.53
8	22.68	37.6	0.00012
9	24.84	42.1	0.00032
10	25.25	44.7	0.0068

4.3.3 Correlation of the Mode Shapes (MAC)

Table 4-7 presents the correspondent experimental mode shapes to the first three numerical, as they correlated according to the Modal Assurance Criteria (MAC). The MAC value for the first numerical mode is very good (MAC = 0.94), but this is not the case for the other two modes.

Table 4-7 Correlation between experimental and numerical mode shapes

Experimental		Numerical			
Mode	**Artemis [Hz]**	**Mode**	**Diana [Hz]**	**Difference [%]**	**MAC**
1	10.23	**1**	9.91	3.13	0.94
8	22.68	**2**	17.30	23.72	0.39
3	19.19	**3**	17.80	7.24	0.65

4.3.4 Calibration Result

The calibration model **CCF2** is not accepted as the final model because:

- It is much stiffer than the real structure, as the eigen frequency range show.
- The MAC value for the numerical modes 2 is very low.
- It does not corresponds to the real condition of the structure since the section of the pins it not accurate enough (all pins are Type A)

4.4 Calibration Model 3 (CCF3)

4.4.1 Eigenvalue Analysis Data

This third calibration model has exactly the same characteristics as the Model CCF2, except for the section of the Pins which are of Type B (Figure 4-7). Table 4-8 contains a summary of the analysis data. The finite element mesh contains 2126 nodes and 1177 elements.

Table 4-8 Eigenvalue analysis data

CCF3	Connections	Damage	Sections	E [GPa]	ν	ρ [kgr/m^3]
Ferramenta	Rigid	Yes	Constant	185	0.25	7750
Grille	Rigid	Yes	Constant	185	0.25	7750
Pins	Rigid	Yes	Type B	185	0.25	7750

4.4.2 Eigen Frequencies

Table 4-9 compares the frequencies between the experimental and the numerical results. The change of the Pins sections did not have remarkable effect on the range of the frequencies and the numerical model remains much stiffer than the experimental one. The first mode remains the one with the higher modal participation mass percentage in the eigenvalue analysis.

Table 4-9 Comparison of the experimental and numerical results

	Experimental	Numerical	
Mode	**Artemis [Hz]**	**Diana – CCF3 [Hz]**	**Modal Participation Mass [%]**
1	10.23	10.00	45.28
2	12.85	17.55	0.0137
3	14.77	18.03	0.0038
4	16.51	25.44	0.0217
5	19.19	32.39	2.750
6	19.80	34.50	6.078
7	22.58	36.83	0.640
8	22.68	38.13	0.0347
9	24.84	42.51	0.0024
10	25.25	45.05	0.0045

4.4.3 Correlation of the Mode Shapes (MAC)

Table 4-10 presents the correspondent experimental mode shapes for the first three numerical modes, as they correlated according to the Modal Assurance Criteria (MAC). The MAC value for the first numerical mode is acceptable (MAC = 0.94), unlike the other two modes.

Table 4-10 Correlation between experimental and numerical mode shapes

Experimental		Numerical			
Mode	**Artemis [Hz]**	**Mode**	**Diana [Hz]**	**Difference [%]**	**MAC**
1	10.23	**1**	10.00	2.25	0.94
8	22.68	**2**	17.55	22.62	0.41
5	19.19	**3**	18.03	6.04	0.56

4.4.4 Calibration Result

The calibration model **CCF3** cannot be accepted as the final model because:

- It is much stiffer than the real structure, as the Eigen frequency range show.
- The MAC value for the numerical mode 2 is very low.

4.5 Calibration model 4 (CCF4)

4.5.1 Eigenvalue Analysis Data

This fourth calibration model has exactly the same characteristics of Model CCF3 except one difference. The connections of the pins with the grille bars are considered as semi – rigid. Springs were introduced at these connections in order to make the finite element model more flexible (Figure 4-9). This approach is closer to the reality since the connection of the pins with the grille bars is made with the use of copper wedges and lead putty.

The springs restrain only the translational degrees of freedom of each node (u_x, u_y and u_z) and they do not have any influence on the rotational degrees of freedom. Three springs were introduced in each connection, one in each direction. By inverse fitting, the stiffness values for the springs were specified as:

Transverse direction (Local X and Local Y): K_s = 5 e+06 N/m

Normal direction (Local Z): K_n = 3 e+04 N/m

Table 4-11 contains a summary of the analysis data. The finite element mesh contains 2184 nodes and 1361 elements of which 183 are the spring elements.

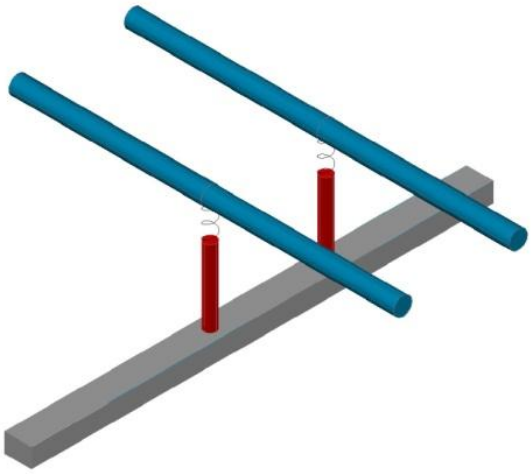

Figure 4-9 Detail of the semi rigid grille – pin connection.

Table 4-11 Eigenvalue analysis data

CCF4	Connections	Damage	Sections	E [GPa]	ν	ρ [kgr/m^3]
Ferramenta	Rigid	Yes	Constant	185	0.25	7750
Grille	Rigid	Yes	Constant	185	0.25	7750
Pins	Semi - Rigid	Yes	Type B	185	0.25	7750

4.5.2 Eigen Frequencies

From the comparison of the experimental with the numerical results (Table 4-12) it is obvious that the numerical model became more flexible after the introduction of the springs. The finite element model has a range of frequencies from 8.35 to 26.75 Hz, which is close to the experimental range (10.23 Hz – 25.25 Hz). The first mode remains the one with the higher modal participation mass percentage in the eigenvalue analysis.

Table 4-12 Comparison of the experimental and numerical results

	Experimental	Numerical	
Mode	**Artemis [Hz]**	**Diana – CCF4 [Hz]**	**Modal Participation Mass [%]**
1	10.23	8.35	43.56
2	12.85	14.77	0.0768
3	14.77	14.95	0.00042
4	16.51	16.28	0.97
5	19.19	20.56	0.016
6	19.80	21.07	0.0025
7	22.58	22.00	0.10
8	22.68	24.87	0.010
9	24.84	24.61	5.01
10	25.25	26.75	0.099

4.5.3 Correlation of the Mode Shapes (MAC)

Table 4-13 presents the correspondent experimental mode shapes to the first three numerical, as they correlated according to the Modal Assurance Criteria (MAC). The MAC value for the first numerical mode is good (MAC = 0.94) and shows that the first experimental coincide with the first numerical mode shape. The MAC value for the other two modes is considered lower but much better than in previous models. It is important to notice that the first numerical frequency differs from the first experimental by 18%. This percentage is considered very high for the first mode which is the most important. A large difference also found between the third numerical mode and the fifth experimental mode (22.09%).

Table 4-13 Correlation between experimental and numerical mode shapes

Experimental		Numerical			
Mode	**Artemis [Hz]**	**Mode**	**Diana [Hz]**	**Difference [%]**	**MAC**
1	10.23	**1**	8.35	18.38	0.94
3	14.77	**2**	14.77	0.00	0.60
5	19.19	**3**	14.95	22.09	0.58

4.5.4 Calibration Result

The calibration model **CCF4** cannot be accepted as the final model because:

- The first numerical frequency (8.35 Hz), which has the higher modal participation mass percentage, differs from the first experimental (10.2 Hz) per 18.38%.

4.6 Calibration Model 4B (CCF4B)

4.6.1 Eigenvalue Analysis Data

The calibration model 5 (CCF4B) is a clone of the calibration model 4 (CCF4) with the only difference located in the Young's Modulus. In this analysis the value of E is increased from 185 GPa to 220 GPa, in order to increase the value of the first frequency of the latter model. Table 4-14 contains a summary of the analysis data. The finite element mesh contains 2184 nodes and 1361 elements of which 183 are the spring elements.

Table 4-14 Eigenvalue Analysis Data

CCF4B	Connections	Damage	Sections	E [GPa]	ν	ρ [kgr/m^3]
Ferramenta	Rigid	Yes	Constant	220	0.25	7750
Grille	Rigid	Yes	Constant	220	0.25	7750
Pins	Semi - Rigid	Yes	Type B	220	0.25	7750

4.6.2 Eigen Frequencies

From the comparison of the experimental with the numerical results (Table 4-15), it is evident that the numerical model became stiffer after the increase of the Young's Modulus. Furthermore, the frequencies range between experimental and numerical models is very similar. The first mode's frequency is 9.06 Hz and remains the one with the higher modal participation mass percentage in the eigenvalue analysis.

Table 4-15 Comparison of the experimental and numerical results

	Experimental	Numerical	
Mode	**Artemis [Hz]**	**Diana – CCF4B [Hz]**	**Modal Participation Mass [%]**
1	10.23	9.06	43.27
2	12.85	15.85	0.265
3	14.77	16.12	0.0063
4	16.51	16.79	1.007
5	19.19	21.78	0.0164
6	19.80	22.48	0.00295
7	22.58	23.04	0.0408
8	22.68	25.71	0.0566
9	24.84	26.43	4.764
10	25.25	28.31	0.0943

4.6.3 Correlation of the Mode Shapes (MAC)

Table 4-16 presents the correspondent experimental mode shapes to the first three numerical, as they correlated according to the Modal Assurance Criteria (MAC). The first numerical mode (f = 9.06 Hz) corresponds to the experimental mode 1 (f = 10.23 Hz) with MAC=0.93 (Figure 4-10, Figure 4-11). The difference of their frequencies is 11.44%, clearly smaller than the analysis with the decreased Young's Modulus.

The second numerical mode (f = 15.85 Hz) corresponds to the third experimental mode (f=14.77 Hz) with MAC 0.5 (Figure 4-12). Their difference of their frequencies is 7.31%.

Finally the third numerical mode (f =16.12) correlates with the fifth experimental mode (f = 19.19 Hz) with MAC = 0.57 (Figure 4-13). The difference of their frequencies is 16%.

Table 4-16 Correlation between experimental and numerical mode shapes

Experimental		Numerical			
Mode	**Artemis [Hz]**	**Mode**	**Diana [Hz]**	**Difference [%]**	**MAC**
1	10.23	**1**	9.06	11.44	0.93
3	14.77	**2**	15.85	7.31	0.51
5	19.19	**3**	16.12	16.00	0.57

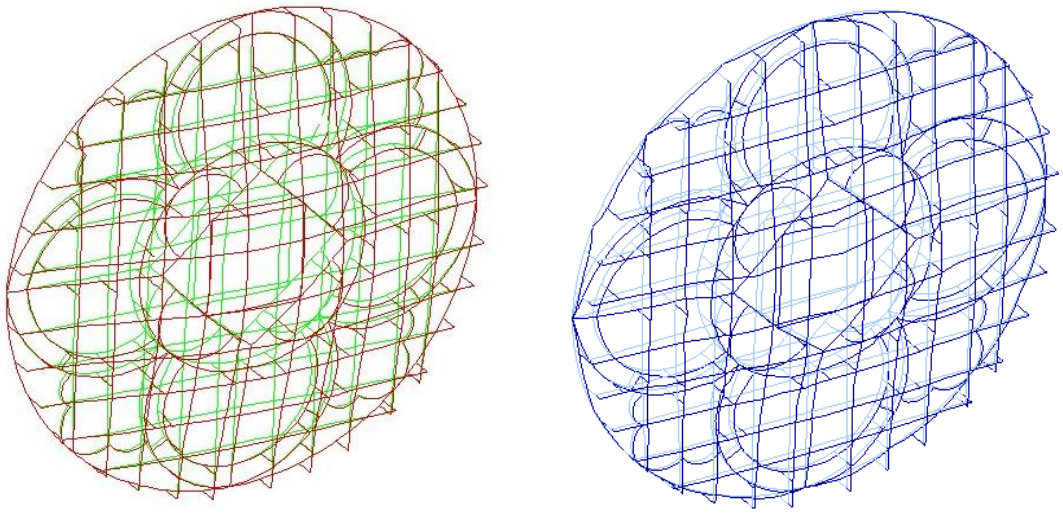

(a) (b)

Figure 4-10 (a) 3D view of the 1st Numerical mode shape (f=9.06 Hz) – (b) 3D view of the 1st experimental mode shape (f=10.23 Hz)

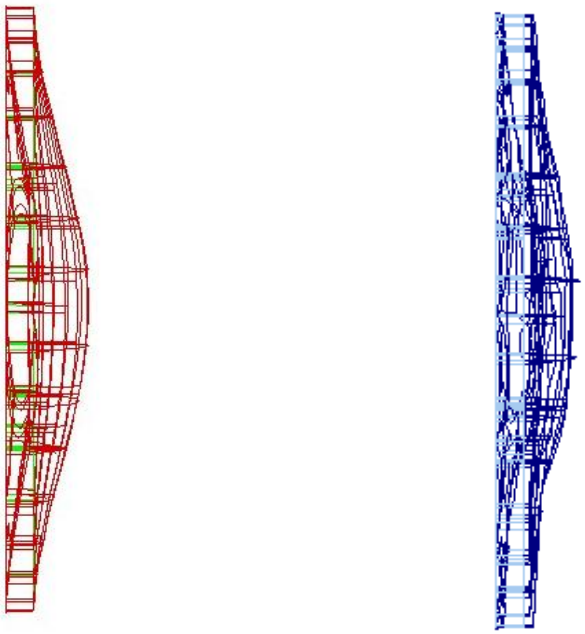

(a) (b)

Figure 4-11(a) Side view of the 1st Numerical mode shape (f=9.06 Hz) – (b) Side view of the 1st experimental mode shape (f=10.23 Hz)

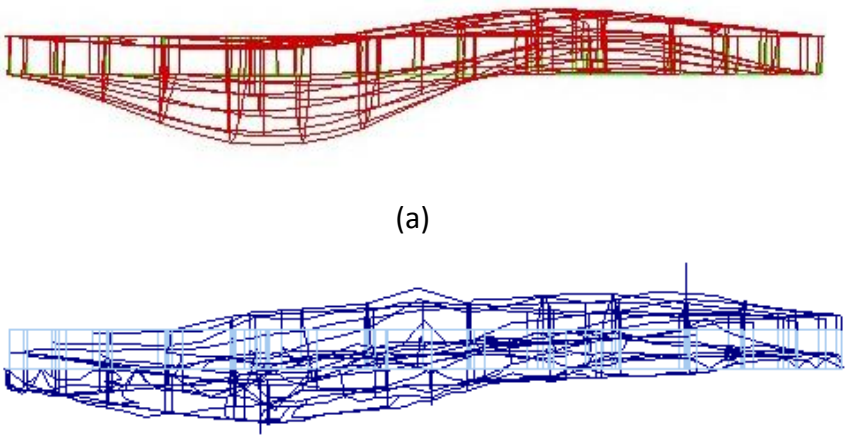

(a)

(b)

Figure 4-12 (a) Top view of the 2nd Numerical mode shape (f = 15.85 Hz) – (b) Top view of the 3rd Experimental mode shape (f = 14.77 Hz)

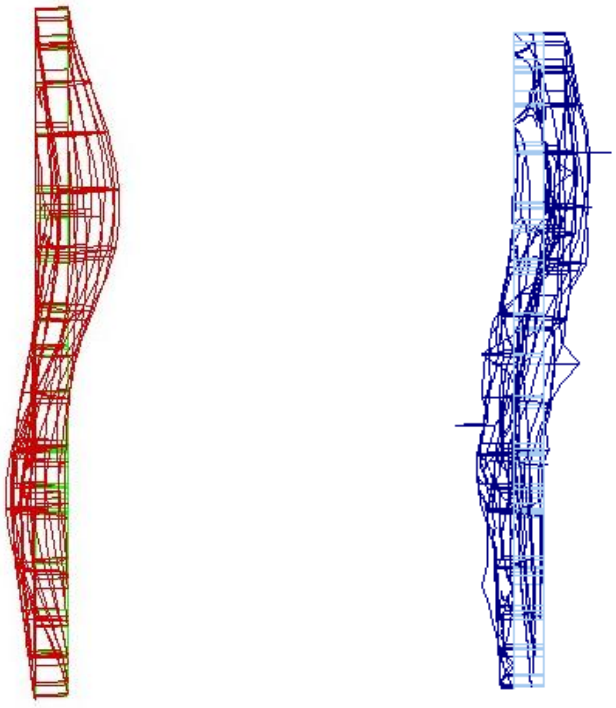

(a) (b)

Figure 4-13 (a) Side view of the 3rd Numerical mode shape (f = 16.12 Hz) – (b) Side view of the 5th Experimental mode shape (f = 19.19 Hz)

4.6.4 Calibration Result

The calibration model **CCF4B** could be accepted as the final model because:

- The frequencies range among the experimental (10.23 – 25.25 Hz) and the numerical (9.06 – 28.31 Hz) model is very similar.
- The first numerical mode (f = 9.06 Hz) corresponds to the experimental mode 1 (f = 10.23 Hz) with MAC=0.93.

4.7 Calibration Model 5 (CCF5)

4.7.1 Eigenvalue Analysis Data

In this calibration model, springs are also introduced in the connections of the horizontal with the vertical grille bars (Figure 4-14). This approach is followed in order to include the wedges – putty connection method of these structural members, in the analysis. Table 4-17 summarizes the eigenvalue analysis data. The finite element mesh contains 2278 nodes and 1648 elements of which 381 are the spring elements.

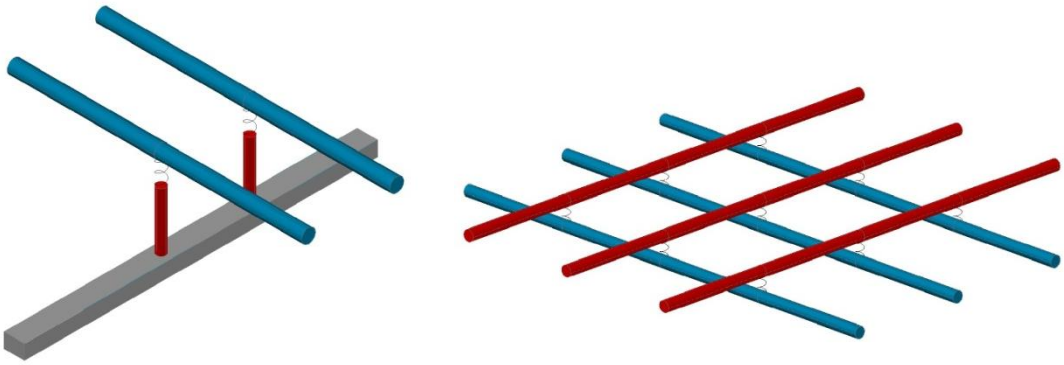

Pins – Grille Bars Horizontal – Vertical Grille Bars

Figure 4-14 Semi - rigid connections considered in the Calibration model 6

Table 4-17 Eigenvalue analysis data

CCF8	Connections	Damage	Sections	E [GPa]	ν	ρ [kgr/m^3]
Ferramenta	Rigid	Yes	Constant	220	0.25	7750
Grille	Semi – Rigid	Yes	Constant	220	0.25	7750
Pins	Semi - Rigid	Yes	Type B	220	0.25	7750

The springs restrain only the translational degrees of freedom of each node (u_x, u_y and u_z) and they do not have any influence on the rotational degrees of freedom. Three springs were introduced in each connection, one in each direction. Table 4-18 presents the stiffness of the springs, as it was specified after trial numerical analyses.

Table 4-18 Springs Stiffness values

	Normal Stiffness K_n [N/m]	Transverse Stiffness K_s [N/m]
Pins	4.00 e+04	5.00e+06
Grille Bars	1.00e+06	5.00e+06

4.7.2 Eigen Frequencies

Table 4-19 compares the first ten eigen frequencies between the experimental and the numerical model. The finite element model has a range of the frequencies from 8.96 Hz to 29.31 Hz that is close to the experimental range (10.23 Hz – 25.25 Hz). The first mode remains the one with the higher modal participation mass percentage in the eigenvalue analysis (43.54%).

Table 4-19 Comparison of the experimental and numerical results

	Experimental	Numerical	
Mode	**Artemis [Hz]**	**Diana – CCF5 [Hz]**	**Modal Participation Mass [%]**
1	10.23	8.96	43.54
2	12.85	15.82	0.050
3	14.77	16.01	0.00021
4	16.51	18.13	1.150
5	19.19	21.66	0.040
6	19.80	23.10	0.018
7	22.58	24.15	0.630
8	22.68	25.77	3.700
9	24.84	26.09	0.266
10	25.25	29.31	0.037

4.7.3 Correlation of the Mode Shapes (MAC)

Table 4-20 presents the correspondent experimental mode shapes to the first three numerical modes, as they correlated according to the Modal Assurance Criteria (MAC). The first numerical mode (f = 8.96 Hz) corresponds to the experimental mode 1 (f = 10.23 Hz) with MAC=0.94 (Figure 4-15, Figure 4-16). The difference of their frequencies is 12.41%.

The second numerical mode (f = 15.82 Hz) corresponds to the third experimental mode (f=14.77 Hz) with MAC 0.66 (Figure 4-17). The difference of their frequencies is 7.11%

Finally the third numerical mode (f =16.01) correlates with the fifth experimental mode (f = 19.19 Hz) with MAC = 0.61 (Figure 4-18). The difference of their frequencies is 16.57%

From the inspection of the results it is evident that after the introduction of the springs at the grille connections of the numerical model, higher MAC values are achieved while the difference between the numerical and experimental frequencies remains the same.

Table 4-20 Correlation between experimental and numerical mode shapes

Experimental		Numerical			
Mode	**Artemis [Hz]**	**Mode**	**Diana [Hz]**	**Difference [%]**	**MAC**
1	10.23	**1**	8.96	12.41	0.94
3	14.77	**2**	15.82	7.11	0.66
5	19.19	**3**	16.01	16.57	0.61

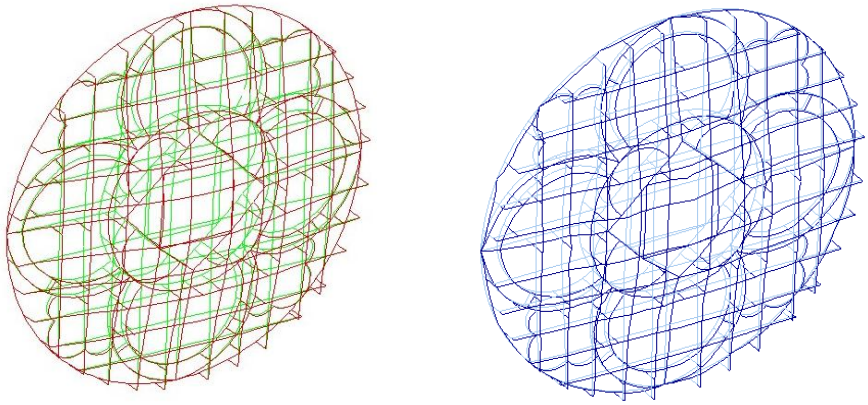

(a) (b)

Figure 4-15 (a) 3D view of the 1st Numerical mode shape (f=8.96Hz) – (b) 3D view of the 1st experimental mode shape (f=10.23Hz)

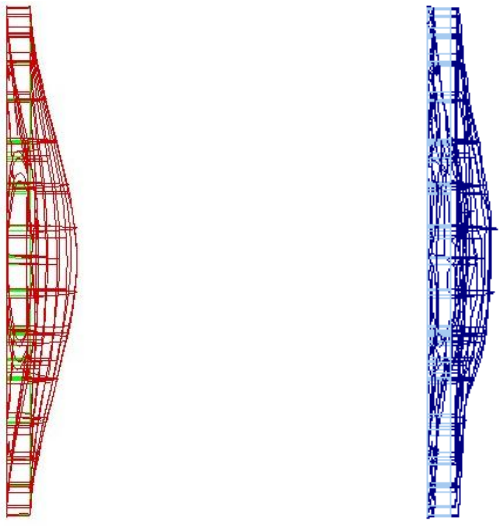

(a) (b)

Figure 4-16 (a) Side view of the 1st Numerical mode shape (f=8.96Hz) – (b) Side view of the 1st experimental mode shape (f=10.23Hz)

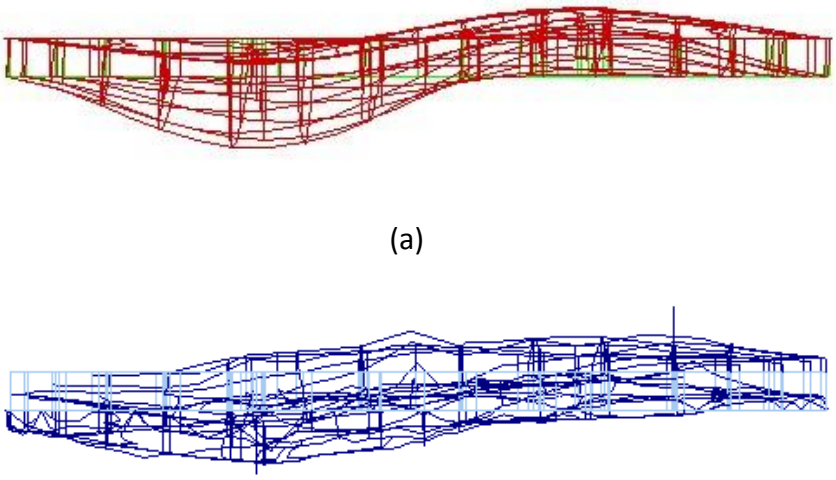

(a)

(b)

Figure 4-17 (a) Top view of the 2nd Numerical mode shape (f=15.82Hz) – (b) Top view of the 3rd Experimental mode shape (f=14.77Hz)

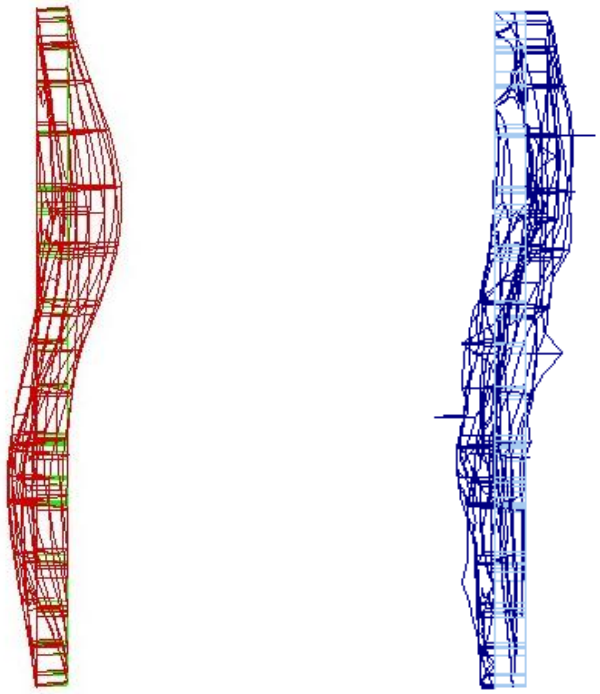

(a) (b)

Figure 4-18 (a) Side view of the 3rd Numerical mode shape (f=16.01Hz) – (b) Side view of the 5th Experimental mode shape (f=19.19Hz)

4.7.4 Calibration Result

The calibration model **CCF5** could be accepted as the final model because:

- The frequencies range among the experimental (10.23 – 25.25 Hz) and the numerical (8.96 – 29.31 Hz) model is very similar.
- The first numerical mode (f = 8.96 Hz) corresponds to the experimental mode 1 (f = 10.23 Hz) with MAC=0.94.
- The MAC values for the second and third numerical modes are the highest achieved during all the calibration procedure.

4.8 Conclusions

From the comparison of the two numerical models CCF4B and CCF5 (Table 4-21), the finite element model **CCF5** is considered as the final model. This model will be used for the future analyses of the structure and was selected for the following reasons:

1. Both numerical models present approximately the same range of eigen frequencies which is very close to the experimental results.
2. The frequency divergence of the first three numerical modes from the corresponding experimental is approximately the same for both finite element models.
3. Both models present approximately the same MAC value for the first mode
4. Model CCF8 presents clearly bigger MAC value for the second and third mode.

Table 4-21 Comparison between CCF4B and CCF5 numerical models

	Numerical Frequency [Hz]	Artemis Frequency Divergence [%]	MAC
CCF4B	9.06 – 28.31		
Mode1	9.06	11.44	0.93
Mode2	15.85	7.31	0.51
Mode3	16.12	16.00	0.57
CCF5	8.96 – 29.31		
Mode1	8.96	12.41	0.94
Mode2	15.82	7.11	0.66
Mode3	16.01	16.57	0.61

Some reasons to justify the divergence between numerical and experimental eigenmodes, particularly, with respect to the lower frequency found numerically for the first mode, are:

1. The use of beam elements instead of 3-D elements, which do not consider correctly the node stiffness due to the finite geometry of the actual node.
2. The absence of the stained glass in the finite element model and by consequence of the additional stiffness that it gives to the Ferramenta members.
3. The consideration of zero rotational flexural stiffness between the pins and the grille.

In addition, it is also noted that the geometry is approximated from the true geometry, by using averaged sections.

Finally it is important to notice that the boundary conditions are not critical for the results since the modal analysis of a finite element model with released rotational degrees of freedom resulted in a 5% more flexible model.

5. SAFETY ASSESSMENT AND PARAMETRIC STUDIES

Introduction

In this chapter the Oculus of Canterbury Cathedral is assessed with respect to the wind load. The results of the non linear analysis are compared with the design values of the Eurocode 1 and the safety factor of the structure is calculated. Furthermore, parametric studies are made in order to investigate the influence of the grille, the damage and the future deterioration on the safety of the structure.

5.1 Wind Load Calculation according to EC1

Figure 5-1 presents the distribution of the wind load on the south - east Transept of Canterbury Cathedral, as it was calculated according to the Eurocode 1 (Tubman, et al. 2010). The corresponding net wind pressure on the Oculus was calculated to be 1.19 kN/m^2.

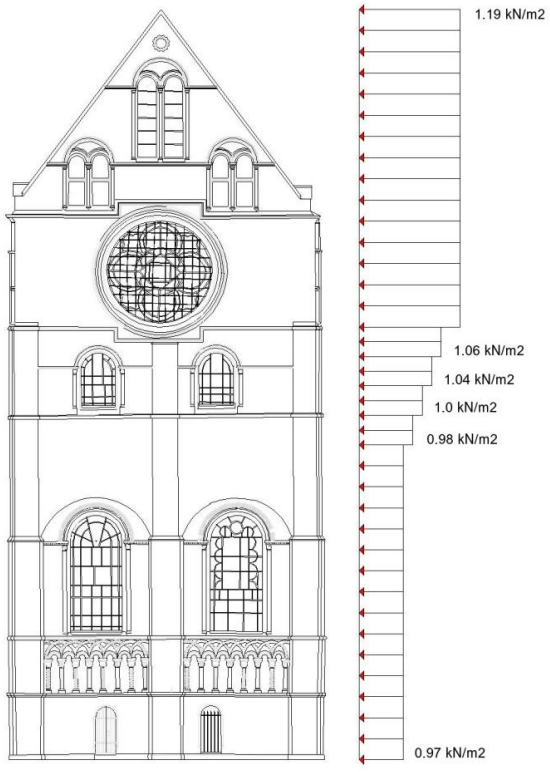

Figure 5-1 Wind load distribution according to the EC1

5.2 Non Linear Properties of Wrought Iron

5.2.1 Wrought Iron Composition

Wrought iron is almost pure iron, with very small carbon content (typically 0 to 0.2%) and a larger amount of silicate slag unalloyed with the iron, which remains after the iron has been worked. This working orientates the slag from globules into strands, which give wrought iron its fibrous fracture. The strands also act as crack – arresters, with the important consequence that wrought iron is ***ductile*** and can undergo substantial deformation before fracture (Bussell 1997).

5.2.2 Stress – Strain Behavior

Wrought iron, like steel, is linear – elastic up to the elastic limit or yield point. It has high elongation at failure (>15%). Figure 5-2 shows a typical stress – strain curve of the wrought iron, based on test results (Bussell 1997).

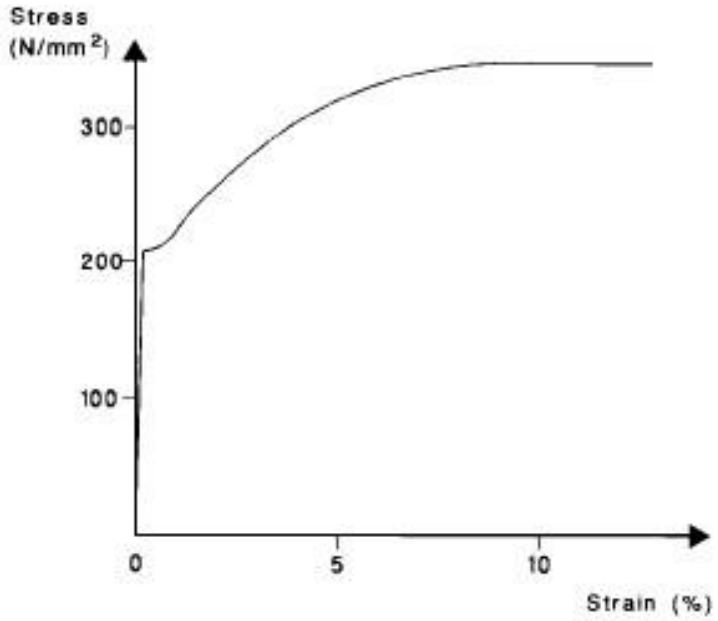

Figure 5-2 Stress – strain curve for a typical wrought iron (Bussell 1997)

In all the non - linear analyses cases, the yield strength of the wrought iron was assumed equal to 180 MPa, a lower end value from (Bussell 1997).

5.3 Present Structure

5.3.1 Analysis data

The "present structure" is considered to be adequately replicated by the finite element model CCF5 (see also chapter 4). Material non – linearity was considered for the wrought iron members (Von Mises), while the springs were assumed elastic. Table 5-1 summarizes the analysis data. The assumed actions were the self weight of the structure and a distributed load of 1 kN/m^2, applied perpendicularly to the Ferramenta.

Table 5-1 Analysis data

	Connections	Damage	Sections	E [GPa]	ν [-]	f_y [MPa]	ρ [kg/m^3]
Ferramenta	Rigid	Yes	Constant	220	0.25	180	7750
Grille	Semi – Rigid	Yes	Constant	220	0.25	180	7750
Pins	Semi - Rigid	Yes	Type B	220	0.25	180	7750

5.3.2 Load – Displacement Diagram

Figure 5-3 presents the variation of the horizontal displacement of the center point of the Ferramenta, as function of the load factor. The structure enters into plasticity for load factor **L.F. = 12.1** e.g. wind load equal to 12.1 kN/m^2. This value, compared with the characteristic value that EC1 proposes for the wind load, gives a safety factor, S.F. = 10.17. Note that very large displacements are found at ultimate stage, which are possibly less reasonable and would require considering non – linear geometrical analysis. Therefore, the actual ultimate load factor will be lower, possibly around 10% (for a displacement about of 0.20 m). Figure 5-4 presents the total and the incremental deformed mesh of the structure at failure.

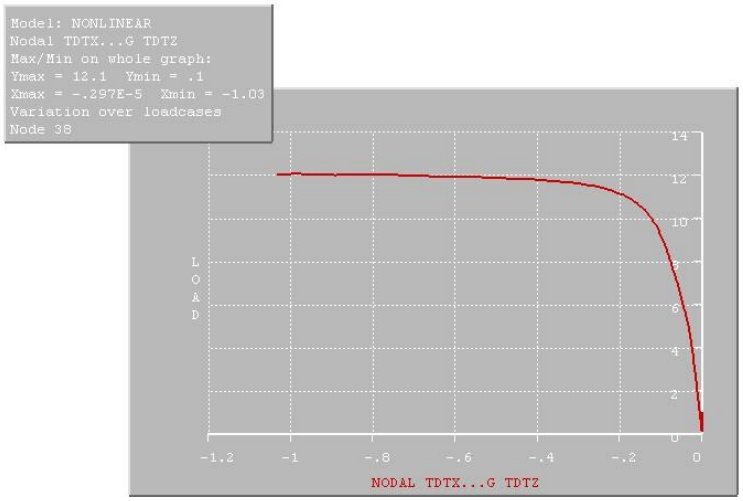

Figure 5-3 Load – Displacement graph

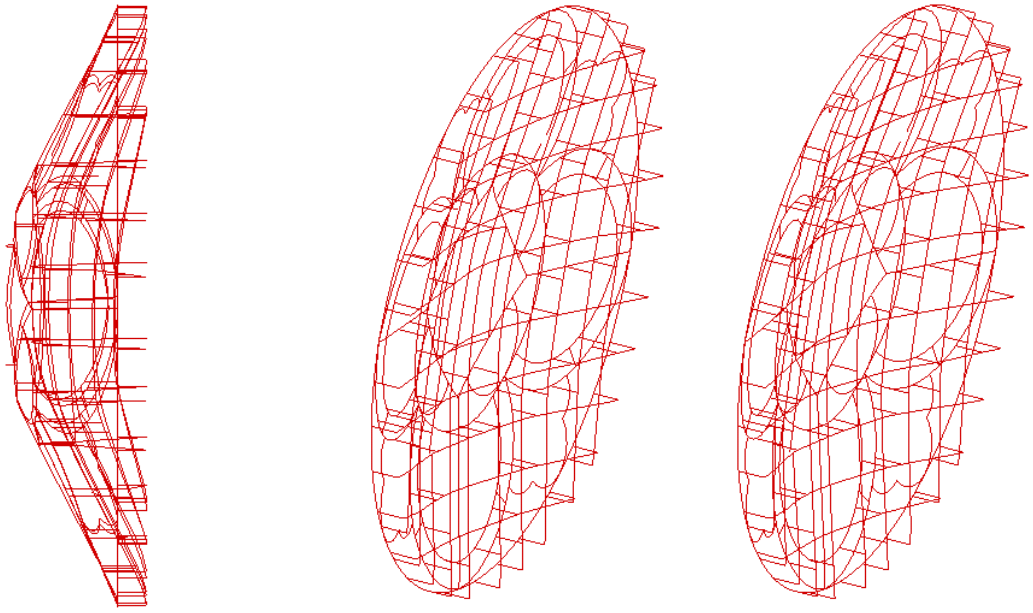

(a) (b)

Figure 5-4 (a) Total deformed mesh - (b) Incremental deformed mesh before and after failure

5.3.3 Yielding

Figure 5-5 presents the developing principal stresses P1. The red color corresponds to the sections were the yield strength is reached (f_y = 180 MPa). Yielding appears in the grille bars (vertical and horizontal) and also in the deteriorated part of some pins.

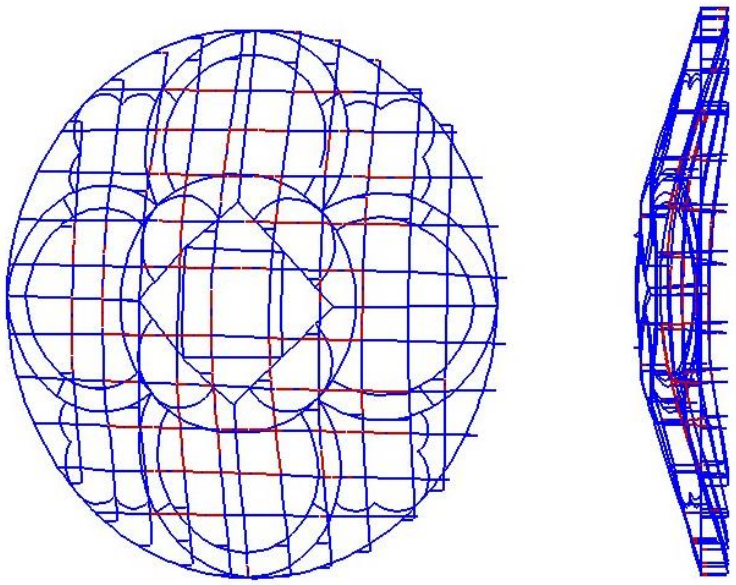

Figure 5-5 Contour plot of the principal stresses P1 (max). The yielded sections are colored red.

5.4 Original Structure

5.4.1 Analysis Data

The "original" structure is considered as the structure just after its construction with no damage or deterioration considered. The finite element model used for this approach is CCF1 (see also chapter 4). Material non – linearity was considered for the wrought iron sections (Von Mises). Table 5-2, presents a summary of the analysis data. Again, the assumed actions were the self weight of the structure and a distributed load 1 kN/m^2, applied perpendicularly to the Ferramenta.

Table 5-2 Analysis data

	Connections	Damage	Sections	E [GPa]	ν [-]	f_y [MPa]	ρ [kg/m^3]
Ferramenta	Rigid	No	Constant	220	0.25	180	7750
Grille	Rigid	No	Constant	220	0.25	180	7750
Pins	Rigid	No	Type A	220	0.25	180	7750

5.4.2 Load – Displacement diagram

Figure 5-6, presents the variation of the total displacement as function of the load factor. The structure enters into the plasticity for load factor **L.F. = 14.2** e.g. wind load equal to 14.2 kN/m^2. This value, compared with the characteristic value that EC1 proposes for the wind load, gives a safety factor, S.F. = 11.93, which is only a moderate increase with respect to the previous analysis.

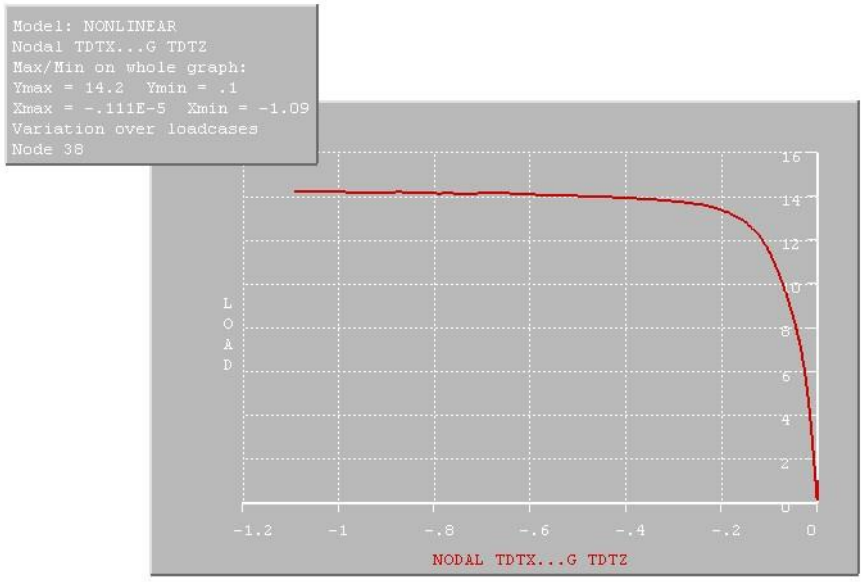

Figure 5-6 Load – Total Displacement graph

5.4.3 Yielding

Figure 5-7 presents the developing principal stresses P1. The red color corresponds to the sections were the yield strength is exceeded (f_y = 180 MPa). It is observed that the majority of the pins are yielded, meaning that failure is now controlled by the pins. This would also suggest that the pins were the most highly stressed parts of the original arrangement, and this could have contributed to accelerating the local breakages once corrosion started reducing the sections. Some of the grille bars also present failure.

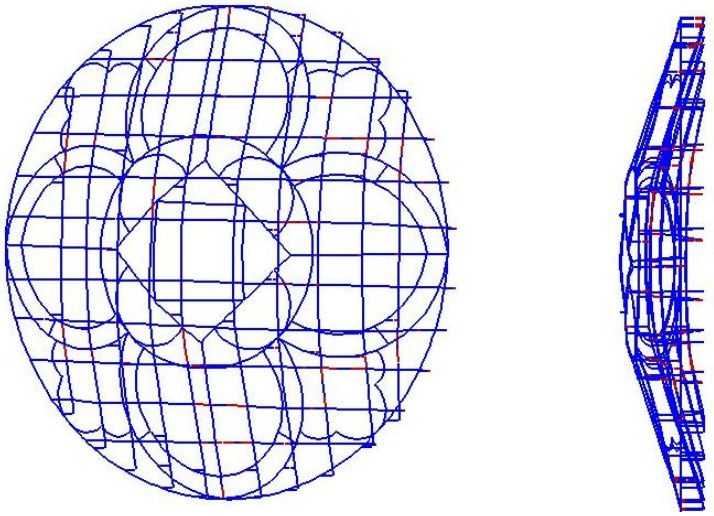

Figure 5-7 Contour plot of the principal stresses P1 (max). The yielded sections are colored red.

5.5 Existing Ferramenta without Grille

5.5.1 Analysis data

In this analysis, the grille and the pins were removed from the finite element model, in order to assess the behavior of the existing ferramenta under wind load, without taking into account the possible influence of the grille. Material non – linearity was considered for the wrought iron sections (Von Mises total plasticity criterion). Table 5-3 presents a summary of the analysis data. Again, the assumed actions were the self weight of the structure and a distributed load of 1 kN/m^2, applied perpendicularly to the Ferramenta.

Table 5-3 Analysis data

	Connections	Damage	Sections	E [GPa]	ν [-]	f_y [MPa]	ρ [kg/m^3]
Ferramenta	Rigid	Yes	Constant	220	0.25	180	7750

5.5.2 Load – Displacement diagram

Figure 5-8 presents the variation of the displacement as function of the load factor. The structure becomes fully plastic for a load factor **L.F. = 8.04** e.g. wind load equal to 8.04 kN/m^2. This value, compared with the characteristic value that EC1 proposes for the wind load, gives a safety factor, S.F. = 6.75, which clearly indicates a significant contribution of the grille to the safety of the structure.

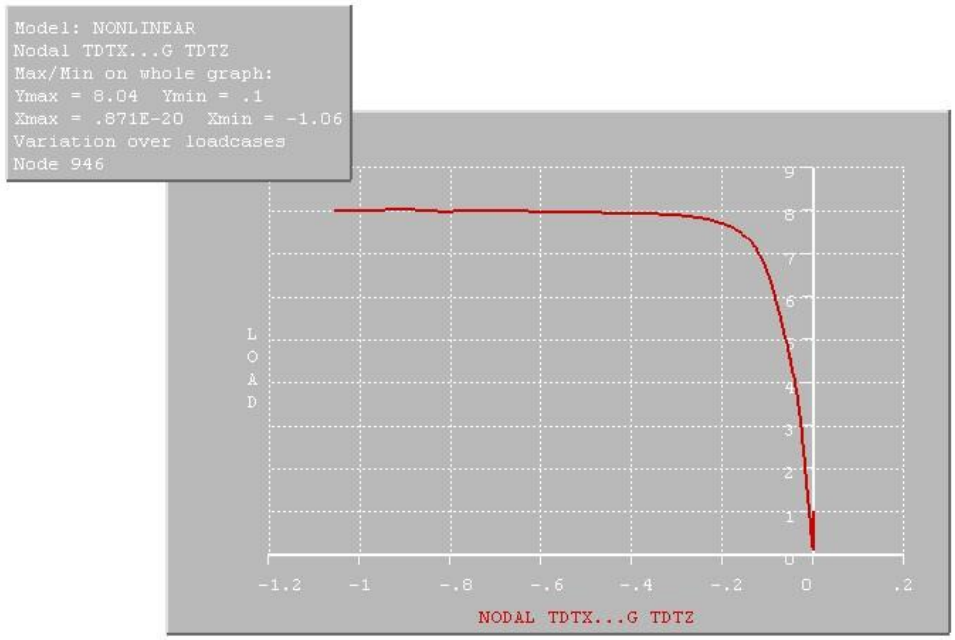

Figure 5-8 Load – Displacement graph

5.5.3 Yielding

Figure 5-9 presents the developing maximum principal stresses P1. Red color corresponds to the sections were the yield strength is exceeded (f_y = 180 MPa). It is observed that failure occurs near the primary fixing points of the Ferramenta.

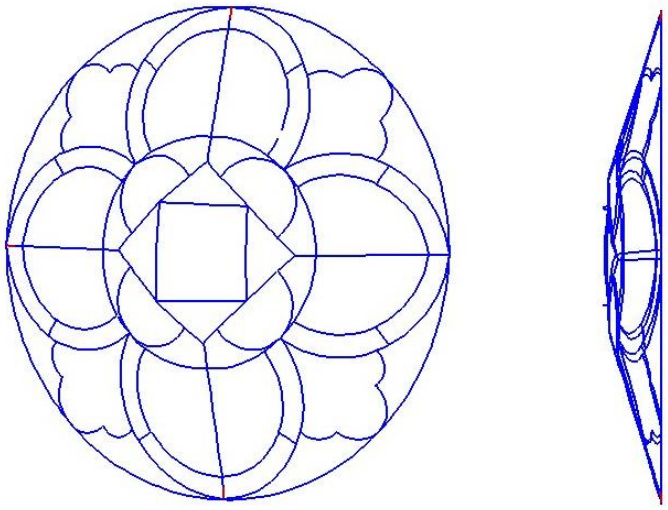

Figure 5-9 Contour plot of the principal stresses P1 (max). The yielded sections are colored red

5.6 Existing Structure considering General Decay

5.6.1 Analysis data

The aim of this analysis is to investigate the influence of a possible future deterioration in the safety of the structure with 50% reduction of the already deteriorated sections and 25% of the sections in good condition.

Material non – linearity was considered for the wrought iron sections (Von Mises total plasticity criterion). Table 5-4 contains a summary of the analysis data. Again, the assumed actions were the self weight of the structure and a distributed load of 1 kN/m^2, applied perpendicular to the Ferramenta.

The decay was considered to affect all the components of the Oculus and was included into the finite element model by reducing their cross – sections. It was assumed that the deteriorated parts will decay faster than the others (Table 5-5).

Table 5-4 Analysis data

	Connections	Damage	Sections	E [GPa]	ν [-]	f_y [MPa]	ρ [kg/m^3]
Ferramenta	Rigid	Yes	Constant Reduced	220	0.25	180	7750
Grille	Semi – Rigid	Yes	Constant Reduced	220	0.25	180	7750
Pins	Semi - Rigid	Yes	Type B Reduced	220	0.25	180	7750

Table 5-5 Cross section reduction [%]

	Ferramenta	Grille	Pins (Type A)	Pins (Type B)	
				Non Deteriorated	Deteriorated
Cross Section Reduction [%]	25	25	25	25	50

5.6.2 Load – Displacement diagram

Figure 5-10 presents the variation of the displacement as function of the load factor. The structure becomes fully plastic for load factor **L.F. = 5.01** e.g. wind load equal to 5.01 kN/m^2. This value, compared with the characteristic value that EC1 proposes for the wind load, gives a safety factor, S.F. = 4.21, which is already a moderately low value if a partial safety factor of 1.5 is considered for the loads and a partial safety factor of 1.5 is considered for the material.

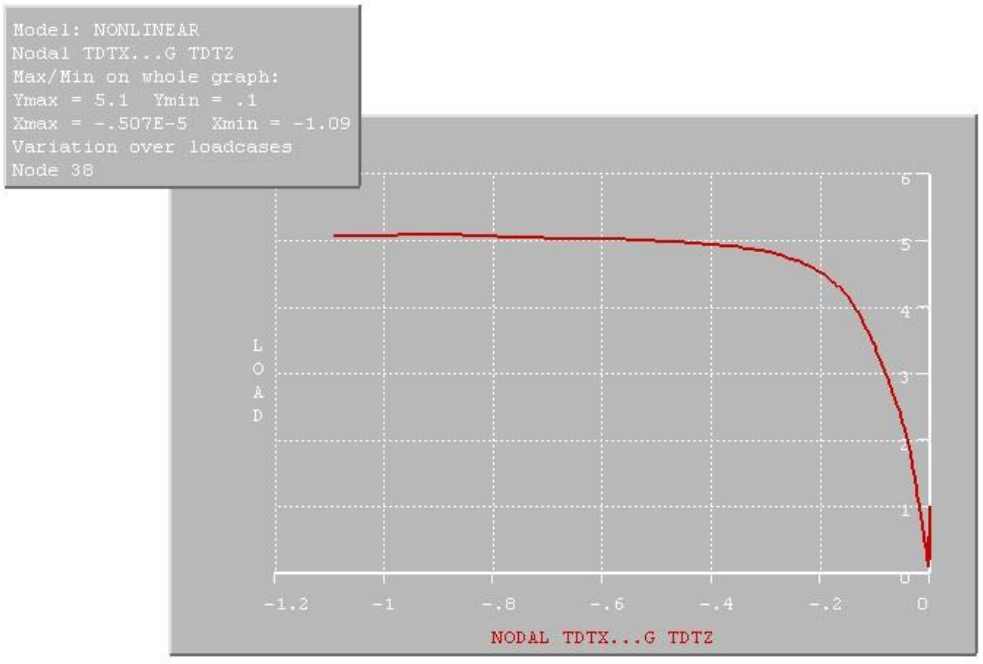

Figure 5-10 Load – Displacement graph

5.6.3 Yielding

Figure 5-11 presents the developing principal stresses P1. The red color corresponds to the sections were the yield strength is exceeded (f_y = 180 MPa). Yielding appears both to the ferramenta and the grille bars (vertical and horizontal) and also to the deteriorated part of the Type B pins.

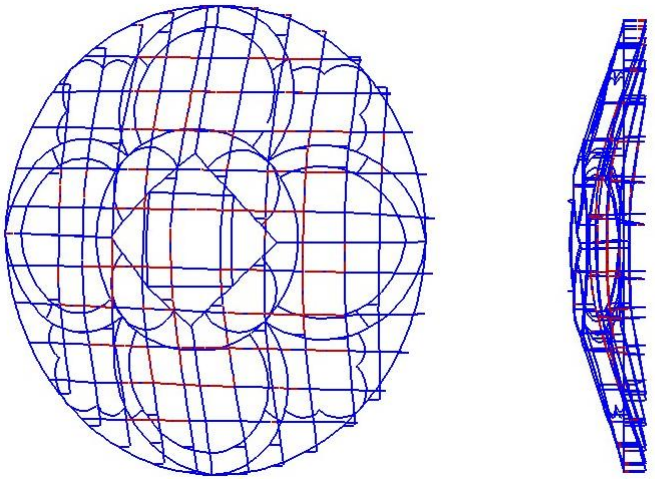

Figure 5-11 Contour plot of the principal stresses P1 (max). The yielded sections are colored red

5.7 Existing Structure considering Decay only to the Deteriorated Parts

5.7.1 Analysis data

The assumption of this analysis was that the decay will happen only to the parts of the structure which are already deteriorated (Type B Pins), while the others will stay as is. Three cases were studied with 25, 50 and 75% reduction of the pins cross section respectively.

Material non – linearity was considered for the wrought iron sections (Von Mises total plasticity criterion). Table 5-6 presents a summary of the analysis data. The assumed actions were the self weight of the structure and a distributed load of 1 kN/m^2, applied perpendicular to the Ferramenta.

Table 5-6 Analysis data

	Connections	Damage	Sections	E [GPa]	ν [-]	f_y [MPa]	ρ [kg/m^3]
Ferramenta	Rigid	Yes	Constant	220	0.25	180	7750
Grille	Semi – Rigid	Yes	Constant	220	0.25	180	7750
Pins	Semi - Rigid	Yes	Type B Reduced	220	0.25	180	7750

5.7.2 Load – Displacement diagram

Table 5-7 and Figure 5-12 present the load factors of the existing structure for different percentages of decay at the deteriorated pins. Both load and safety factor values are decreasing as the decay percentage is increasing, as expected. Still a high safety factor is found for all analyses[2].

Table 5-7 Load and safety factors

	Existing	Decay 25%	Decay 50%	Decay 75%
Load Factor	12.1	12.05	11.9	11.42
Safety Factor	10.17	10.12	10	9.60

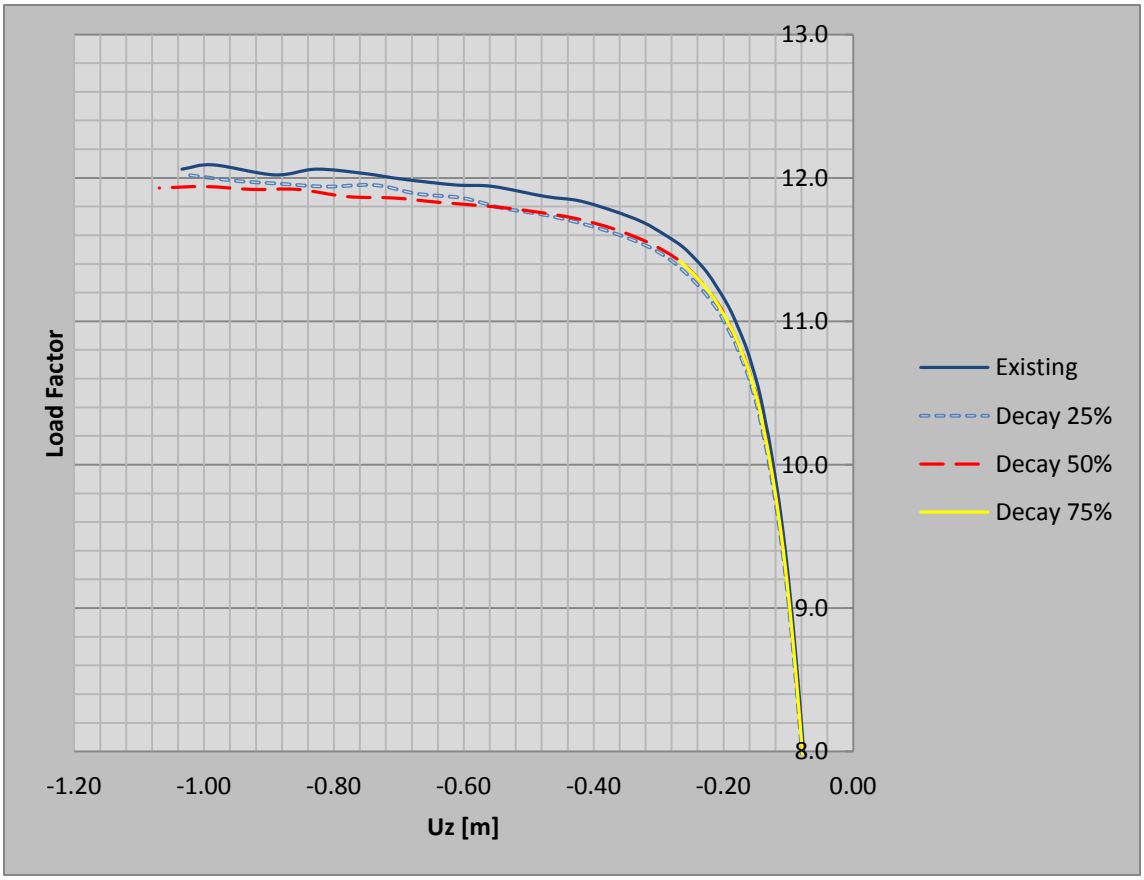

Figure 5-12 Load – Total Displacement graph

[2] Note that the analysis with a decay of 75% was stopped due to divergence and the actual failure load is higher than reported.

5.7.3 Yielding

Figure 5-13, compares the developing principal stresses P1 between the Existing model and the most deteriorated analysis case (Decay 75%). An increment of the sections which yield is observed.

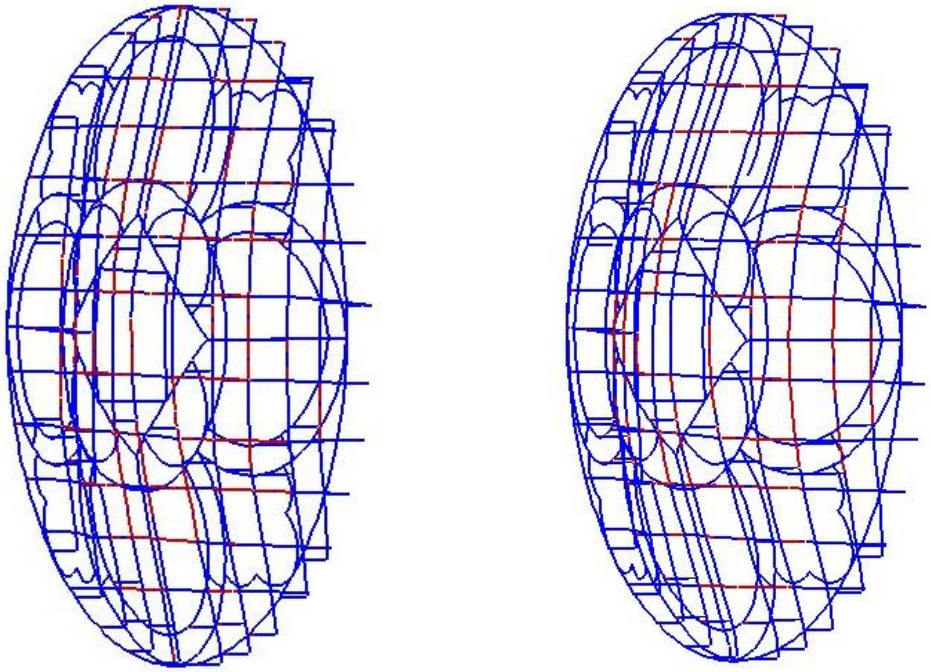

Existing Structure 75% Decay

Figure 5-13 Contour plot of the principal stresses P1 (max). The yielded sections are colored red

5.8 Conclusions

Table 5-8 and Figure 5-14 present a summary of the results of all the non - linear analyses cases carried out for the safety assessment of the Oculus against wind loading. Figure 5-15 compares the safety factors obtained from the numerical models with the safety factor provided from EC1.

Table 5-8 Summary of the Non – Linear analyses results

	Present	Original	No Grille	Decay 25%	Decay 50%	Decay 75%	Gen. Decay
L.F.	12.10	14.2	8.04	12.05	11.90	11.42	5.01
S.F.	10.17	11.93	6.75	10.12	10.00	9.60	4.21

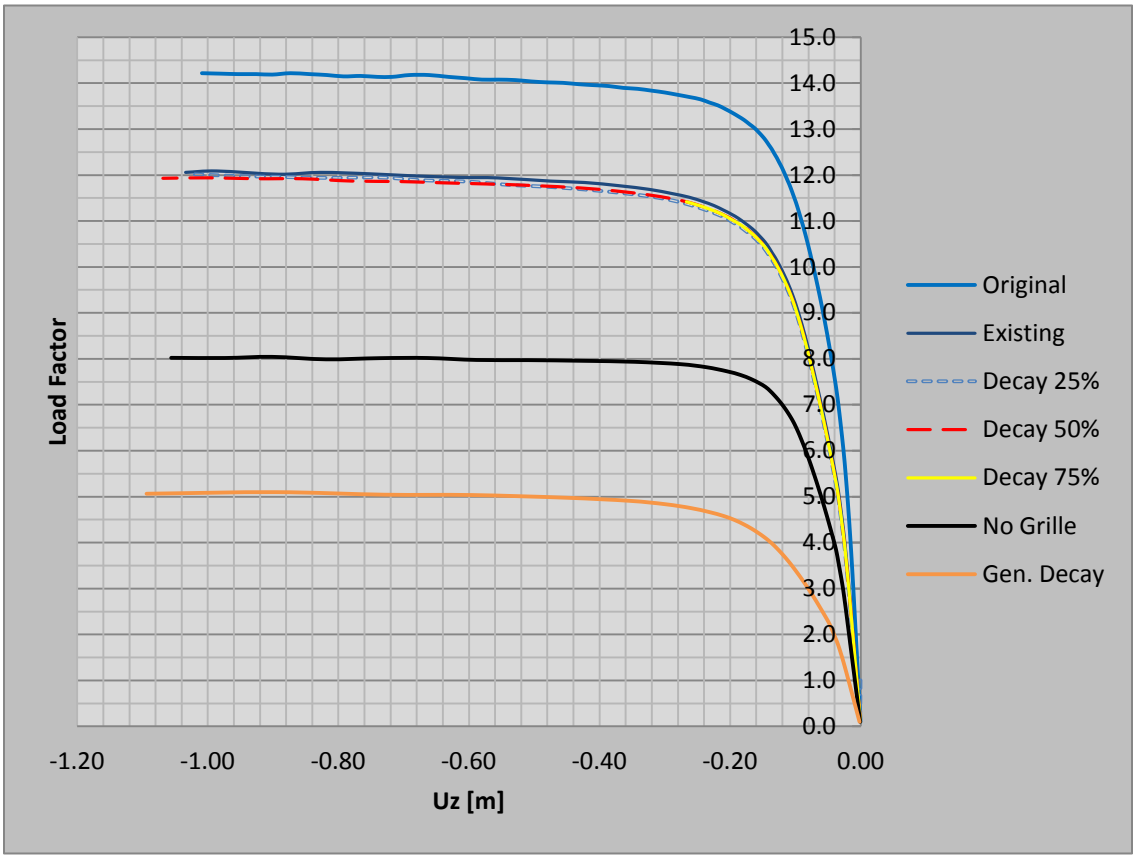

Figure 5-14 Load – Displacement diagram of all the Non – Linear analysis cases

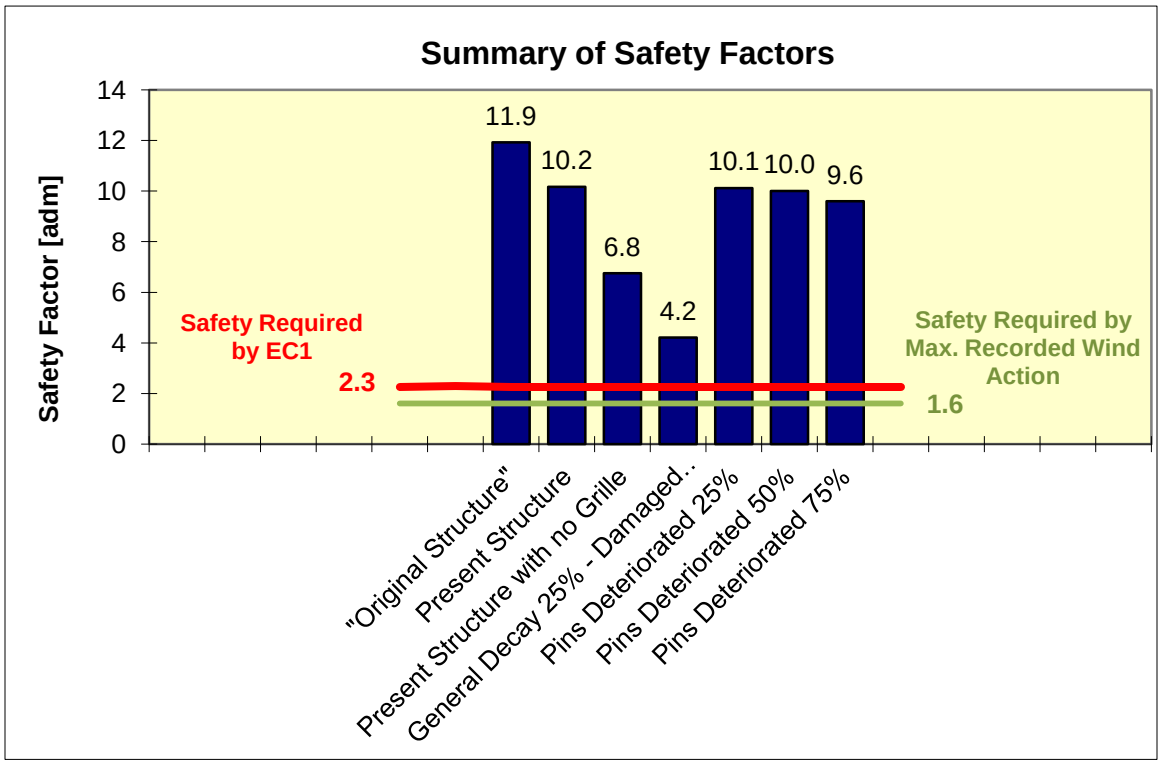

Figure 5-15 Summary of the Safety Factors

The following conclusions are possible:

- By comparing the existing structure as it stands today with the original, the Oculus could sustain 15% more wind load in its initial condition than now.
- The analysis of the existing Oculus with the Ferramenta and no Grille shows that the structure in this configuration could sustain 33.6 % less wind load than before. The Grille therefore provides around one third of the total strength.
- The parametric study of the possible future decay of the deteriorated part of the pins (assuming that these lose up to 75% of their cross – section), shows that the safety factor of the structure would drop of a maximum 5.6%. This suggests that the sections presently showing signs of decay are already providing a very limited contribution to the global stability of the Oculus.
- The result of a future general deterioration affecting the entire structure and causing a loss of cross section of 50% to the decayed areas and 25% to the rest of the structure would cause a 58% loss of the wind load bearing capacity of the Oculus. This suggests that a general future corrosion affecting the whole Oculus would affect the global behavior much more than localized damages to the pins.
- It is worth stressing that in all these cases the safety of the Oculus against wind loading seems guaranteed and is still above the requirements of the Eurocode 1.

6. CONCLUSIONS OF THE THESIS

In this dissertation, many concepts covered by the "Structural Analysis of Monuments and Historical Constructions" Master Course were applied in order to assess the safety of the South Oculus at Canterbury Cathedral. The following points summarize the key aspects of the Thesis and also highlight the most important conclusions arising from this work:

- The South Oculus at Canterbury Cathedral is a wrought iron space frame, consisting of two layers (Ferramenta and Grille) connected by tie bars (Pins).
- The in situ survey at the Cathedral revealed that the Ferramenta and the external grille are in general good condition, whereas the tie bars/pins are the most deteriorated part of the structure. Some of them are broken or inactive but the majority of them have suffered serious reduction in their cross - section.
- The calibration of a finite element model simulating such a complex structure can be time consuming and it is a procedure that requires considerable expertise since many parameters affecting the response of the structure are involved (actual geometry, material properties, condition of the connections, adopted model etc).
- The model updating procedure was completed with the conclusion that the connection of the grille bars to each other and to the pins, cannot be assumed as rigid, since the only finite element model that was approaching the experimental result of the ambient vibration test was the one with springs in the afore mentioned connections. This suggests that some relative movements between the parts at these connections can occur.
- The non – linear analysis of the existing structure with respect to the wind load resulted in a safety factor of about ten, when compared with the wind load that the EC1 proposes. The minimum acceptable safety factor expected, considering the partial load safety factor and the partial material safety factor, is in the range of two to three.
- The Oculus in its original condition could sustain 15% more wind load than nowadays, meaning that the deterioration and damage has affected the structure only marginally. This also suggests that repairing the damaged parts is not structurally required and would have a limited impact on the capacity of the structure.
- The external grille is very important for the safety of the structure, since the safety factor is reduced by about one third if the grille is removed. The grille has therefore a clear structural function and contributes to the global stability of the Oculus.
- Severe further deterioration of the presently decayed parts would have very little impact on the global safety of the structure. This suggests that repairing the damaged pins is not strictly required given the redundancy of these.

- A possible further general deterioration of the structure in the very long term (hundreds of years) leading to a cross - section reduction of the deteriorated parts by 50% and a cross - section reduction of the rest by 25%, could cause a drop of up to 60% of the load bearing capacity of the Oculus, still providing a moderately safe condition.
- The parametric analysis of possible future damage scenarios suggests that a general corrosion to the structure leading to a loss of cross section would drastically affect the structural strength of the Oculus, and should therefore be prevented. Long-term monitoring of the state of the corrosive process would allow taking remedial actions in time and also assessing whether the superficial treatment proposed as part of the current restoration has achieved the goal of preserving the fabric and preventing further decay.
- The analysis of the wind monitoring data shows that the maximum wind load recorded at the Cathedral between August 2007 and May 2011 has caused a pressure on the Oculus which is about 70% of the strength required by the EC1. The FE analyses have shown that this pressure is about 16% of the estimated present strength of the structure.

Possible future work could include:

- Investigation about how the space frame was lifted from the ground in order to take its place into the masonry wall and the associated safety assessment, although this seems rather high.
- Definition of the maximum diameter of a glass window that could be supported by a wrought iron space – frame keeping similar cross sections for the Ferramenta and the Grille.
- A stochastic safety assessment of the structure taking into consideration the actual coefficient of variation found in the bars.
- A study of the same structure combined with the additional internal frame which will be built as part of the current restoration in order to introduce protective glazing to the Oculus.

Bibliography

ARTeMIS User's Manual. Structural Vibration Solutions A/S, Release 5.3.

Autocad User's Manual. Autodesk, Release 2010.

Brincker, R., L. Zhang, and P. Andresen. "Modal Identification from Ambient Responses using Frequency Domain Decomposition." *Proceedings of the 18th International Seminar on Modal Analysis.* San Antonio, Texas , 2000.

Bussell, M. *Appraisal of Existing Iron and Steel Structures.* Berkshire: The Steel Construction Institute, 1997.

Collinson, P, N Ramsay, and M Sparks. *A History of Canterbury Cathedral.* The Chapter of the Canterbury Canthedral, 2002.

DIANA User's Manual. TNO DIANA BV, Release 9.4.

Ewins, D. J. *Modal Testing, Theory, Practice and Application.* Baldock, Hertfordshire, England: Research Studies Press LTD, 2000.

Geddes, Jane. *The Ferramenta of the Oculi at Canterbury Cathedral.* 2011.

Hall, Brian. *Canterbury Cathedral, South Oculus, Cleaning Trials.* London: Hall Conservation LTD, 2011.

Newton, H. "Stone repair and conservation after 1945." In *The Architecture of Canterbury Cathedral*, by J Foyle. London: Scala Publishers , 2012.

Peeters, B. *System Identification and Damage Detection in Civil Engineering.* PhD Thesis, Belgium: Catholic University of Leuven, 2000.

Ramos, Jose Luis Ferreira. *Damage Identification on Masonry Structures Based on Vibration Signatures.* 2007.

SAP2000 User's Manual. Computers & Structures inc, Release 14.1.0.

The Canterbury Cathedral Website. www.canterbury-cathedral.org.

Tubman, J, B C Ayres, M G Baker, I W Burgess, D Dibb - Fuller, and R Shipman. *Manual forthe design of building structures to Eurocode 1 and Basis of Structural Design.* London: The Institution of Structural Engineers, 2010.

Vidimus on Line Magazine. 2006. www.vidimus.org.

Willis, R R. *The Architectural History of Canterbury Cathedral.* London, 1845.